ANL-18/35

Second Annual Progress Report on Transmission of Information by Acoustic Communication along Metal Pathways in Nuclear Facilities

Transmission of Information by Acoustic Communication along Metal Pathways in Nuclear Facilities

Nuclear Science and Engineering Division

ANL-18/35

Second Annual Progress Report on Transmission of Information by Acoustic Communication along Metal Pathways in Nuclear Facilities

Transmission of Information by Acoustic Communication along Metal Pathways in Nuclear Facilities

prepared by
Alexander Heifetz[1], Xin Huang[1,2], Roberto Ponciroli[1], Jacey Young[1,3], Dmitry Shribak[1,4], Sasan Bakhtiari[1], Jafar Saniie[2], and Richard B. Vilim[1]

[1]Nuclear Science Engineering Division, Argonne National Laboratory
[2]Department of Electrical and Computer Engineering, Illinois Institute of Technology, Chicago, IL
[3]Department of Physics, St Norbert College,
[4]Department of Physics, University of Chicago, Chicago, IL

September 28, 2018

Table of Contents

List of Figures

List of Tables

Abstract

Transmission of information using elastic waves on existing metallic pipes provides an alternative communication option for a nuclear facility. The advantages of this approach consist of transmitting information through barriers, such as the containment building wall. In this paper, we discuss acoustic communication system design considerations, including data transmission requirements for a nuclear facility and transducer operating conditions. A viable candidate for acoustic communication channel is a chemical volume control system (CVCS) stainless steel pipe, which penetrates through the containment building wall. A laboratory bench-scale system consisting of a nuclear grade CVCS-like pipe and ultrasonic transducers was assembled for a preliminary communication system analysis. Because of low bandwidth and spectral dispersion of ultrasonic transducers, on off keying (OOK) protocol was chosen for data communication. Laboratory tests have shown the acoustic communication system to be resilient to low frequency noise, such as process noise at a nuclear facility. Amplitude shift keying (ASK) communication protocol was developed using GNURadio software environment, and demonstration of data transmission was performed using piezo-electric (PZT) and electromagnetic acoustic (EMAT) transducers. Main achievements thus far include demonstration of transmission of sound and text files with PZT and EMAT across six-foot long nuclear grade stainless steel pipe, and demonstration of image transmission with PZT over the pipe. In the former example, 32KB image was transmitted at data rate of 2KB/s. Efforts are currently under way to further enhance data transmission rate.

1. Introduction

1.1. Background

Integration of advanced communication technologies into nuclear facility operation has the potential for enhancing safety and accident-resiliency of the existing fleet of aging light water reactors, as well those of future advanced reactors (Korsah 2017). Conventional wired and wireless communication systems face implementation challenges at nuclear facilities due to the presence of thick reinforced concrete walls with steel liners throughout much of nuclear facility, especially the containment building. In addition, concerns related to security gaps in conventional communication networks have to be addressed when developing communication systems for nuclear facilities. To address communication technology gaps for nuclear energy, we are currently developing the acoustic communication (AC) hardware and network protocols for efficient and secure transfer of data.

In this report, we describe recent progress on developing a wireless communication system for a nuclear facility, in which information is carried with elastic waves propagating on metallic pipes. Traditionally, elastic wave propagation has been a frequent technique for non-destructive testing (NDT) of steel pipes (Bakhtiari 2018). In the NDT methodology, elastic waves are launched into a steel pipe with an ultrasonic transducer. Material defects comparable in size to wavelength scatter ultrasonic waves, and analysis of scattered signal allows quantifying the defect and its location. As a variation on NDT technology, ultrasonic transducers placed at the ends of a pipe, and operating at wavelengths larger than typical microcrack sizes, can act as a transmitter and receiver of information (Wang 2017). Such communication system would take advantage of the existing piping infrastructure to transmit information in and out of containment building, as shown in Figure 1. (Argonne 2018). Furthermore, information sent over this system would only be accessible through direct physical contact with the pipes, thus establishing a protection layer against unauthorized eavesdroppers.

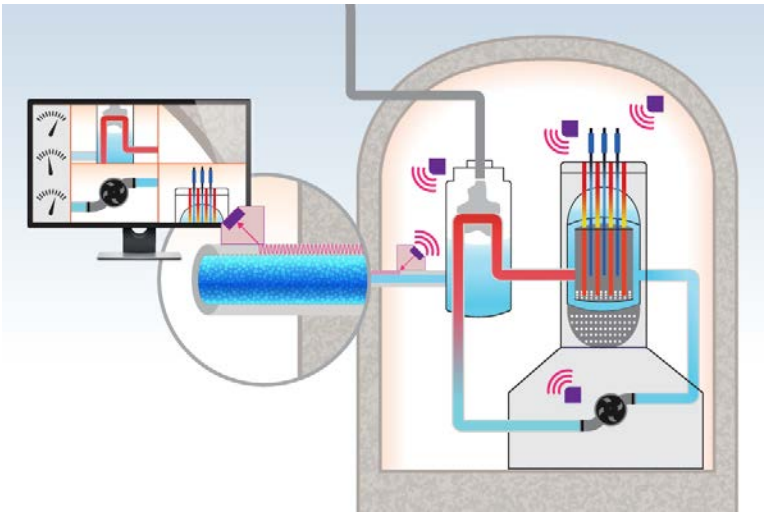

Figure 1 – Proposed acoustic communication system at a nuclear facility would transmit information on steel pipes already in place for nuclear reactor operation (Argonne 2018).

1.2. Introduction

In this project, we are developing a wireless communication system for a nuclear facility, in which information is carried with elastic waves propagating on metallic pipes. Our project combines the fields of acoustics with communication technology. Because of limited bandwidth of ultrasonic transducers, on-off-keying (OOK) digital communication protocol was chosen for information transmission over an acoustic channel (Chakrabory 2015, Heifetz 2017). Current work on the project is focused on investigating communication channel capacity (bit rate or duty cycle of the analog signal amplitude waveform), reliability (bit error rate) and energy efficiency (energy consumption per bit) of OOK. Design considerations of the OOK communication protocol are intimately connected to physical characteristics of the communication channel.

In general, communication data rate is proportional to carrier frequency. However, signal attenuation in the channel due to absorption is proportional to carrier frequency as well, so that carrier frequency cannot be increased indefinitely. Prior work demonstrated that pulse energy fades below detection threshold if the pulse temporal duration is smaller than some limit. Other factors adversely influencing communication bit rate studied more recently include mixture of modes and echoes. Longitudinal and shear waves have different propagation velocities in stainless steel, so that excitation of both modes can lead to bit errors. Excitation of shear waves only can be achieved with EMAT (electromagnetic acoustic transducers). Refracted shear waves can be excited with PZT (piezo-electric transducers) mounted on angled wedge, with an angle larger than the first critical angle. Echoes occur due to reflections of acoustic waves at discontinuities, such as pipe ends. Echoes are stronger at lower frequency, which suffers less attenuation from absorption losses in the channel. In addition, only round-trip echoes, re-scattered in the direction of the original signal, couple into the angled-wedge mounted PZT receiver. On the other hand, EMAT receiver is omnidirectional, and picks up echoes from every scattered in any direction towards the receiver. Thus, longer distance of echo propagation before coupling into receiver makes PZT-based channel more immune to echoes. Some aspects of the communication protocol affecting data bit rate include length of time required to achieve optimal performance with active control gain, and received analog signal decimation procedure.

This report describes implementation of amplitude shift keying (ASK) communication protocol using GNURadio software environment, and evaluation performance of communication channels based on PZT and EMAT transducers. Main achievements thus far include demonstration of transmission of sound and text files with PZT and EMAT across six-foot long nuclear grade stainless steel pipe, and demonstration of image transmission with PZT over the pipe. In the former example, 32KB image was transmitted at data rate of 2KB/s. Efforts are currently under way to further enhance data transmission rate.

2. System Design Considerations

2.1. Transducer operating conditions

Acoustic communication system under development in this project is intended to provide accident-resilient communication option for the nuclear facility. That is, the communication system is expected to operate in normal and post-accident scenarios. As previously described (Heifetz 2017, Heifetz 2018), during an extended station blackout (SBO), the communication unit cannot rely on unlimited power supply. Therefore, we assumed that the only way the acoustic transmission system can be powered is through a battery, such as battery pack of a Tesla Model S (100kWh). To synchronize our efforts with severe accident response R&D, we stipulate that communication system is expected to be used in post-accident reactor monitoring for at least 72 hours.

In general, communication data rate is proportional to carrier frequency. However, signal attenuation in the channel due to absorption is proportional to carrier frequency as well, so that carrier frequency cannot be increased indefinitely. Prior work demonstrated that pulse energy fades below detection threshold if the pulse temporal duration is smaller than some limit. Other factors adversely influencing communication bit rate studied more recently include mixture of modes and echoes. Longitudinal and shear waves have different propagation velocities in stainless steel, so that excitation of both modes can lead to bit errors. Excitation of shear waves only can be achieved with EMAT's. Refracted shear waves can be excited with PZT's mounted on angled wedge, with an angle larger than the first critical angle. Echoes occur due to reflections of acoustic waves at discontinuities, such as pipe ends. Echoes are stronger at lower frequency, which suffers less attenuation from absorption losses in the channel. In addition, only round-trip echoes, re-scattered in the direction of the original signal, couple into the angled-wedge mounted PZT receiver. On the other hand, EMAT receiver is omnidirectional, and picks up echoes from every scattered in any direction towards the receiver. Thus, longer distance of echo propagation before coupling into receiver makes PZT-based channel more immune to echoes. Some aspects of the communication protocol affecting data bit rate include length of time required to achieve optimal performance with active control gain, and received analog signal decimation procedure.

As discussed in the previous reports, the acoustic transmission scheme is going to be installed on a pipe which is associated with the auxiliary systems. As reported in [3,4], the CVCS charging lines inside containment are usually insulated. For example, in the Calvert Cliffs units, the insulation material for the charging line is mineral wool in panels. The panels typically consist of 22 gauge stainless steel sheet, a thickness of 9 pound density mineral wool (corresponding to about 2 inch thickness), and a 24 gauge stainless steel sheet. In addition to being thermal insulator, mineral wool is also a strong attenuator for ultrasonic waves.

All pipes installed in a nuclear unit are sized and certified as compliant with the appropriate ASME codes. Accordingly, once a pressure boundary of pipe is certified, any intervention that might affect its capability to sustain normal operation pressure transients is not allowed. Therefore, any tampering with pipe surface, such as welding and drilling of the pipe is not allowed. On the other hand, there are no explicit statements against locally removing a section of the mineral wool to

allow the installation of transducers. Minimal heating losses would be expected from removal of small section of insulation

The charging line of CVCS (chemical and volume control system) was previously identified as a promising location for the application of an acoustic transmission device. This is because only the charging line offers the combination of two favorable characteristics: a relatively low temperature and containment isolation valves both placed outside containment. These conditions refer to the normal operation. To be conservative, the accidental conditions should be accounted for as well. The acoustic transmission system is expected to be particularly useful when other conventional communication means cannot be used. Therefore, theoretically, the worst accidental scenario conditions (BDBA, Beyond Design Basis Accident) should be accounted for. Otherwise, at this preliminary stage, we will consider DBA (Design Basis Accident) conditions only. The transducers are expected to be applied to the CVCS charging line inside the containment. The components in the primary containment are exposed to the most severe temperature, humidity, and radiation environments. Typical value of environmental stresses of containment isolation (CI) function components inside the PWR containment (Heifetz 2017, Heifetz 2018) are listed in Table 1. We assume that the transducers are subject to the same environmental stresses that are experienced by the CI function components inside the primary containment.

Table 1 – Typical environmental stresses on CI function components

Parameter	Normal	Accident
Temperature	50-120 °F	300 °F
Pressure	atmospheric	70 psig, max
Relative Humidity	30-100 %	100 %
Radiation	50 rads/hr	150 Mrads/hr

Therefore, following DBA conditions, we can assume design temperature of 150 °C, as well as high humidity and elevated ionizing radiation levels for the acoustic transducers operational environment. Given the expected operating conditions, we conclude that despite higher power consumption, EMAT might be preferable for implementation of information transmission system at the power plant. Because of relative simplicity, PZT is used for proof-of-principle communication system development. However, eventual design could consist of EMAT transmitter and receiver.

2.2. Reactor Process Variables and Signals

Estimates of communication system power requirements consist of surveying critical reactor process variables, information on which needs to be transferred outside the containment building in a post-accident scenario. Data requirements for transmitting information from these sensors constitute the minimum set of requirements for a viable communication system at a nuclear facility. Table 2 lists the reactor process variables, and corresponding measurement sensors. These

sensors are characterized by specific time constants, i.e. each sensor has a specific dynamic behavior which will contribute determining the frequency of the transmitted train signals [3,4]. The sensors generate current or voltage signals (mV or mA) that can be converted into the corresponding units of measurement (°C, bar, etc.) before being transmitted. On the other hand, the number of bits corresponding to each one of the monitored variables depends on the desired resolution, which is characteristic of the considered variable. Therefore, the number of dedicated bits does not depend on the features of the sensors under consideration, but on the A/D converter. In common practice, using 24 bits will ensure a very high resolution. Currently, the standard A/D converters use 8-16 bits. For our purposes, as a first guess, we will assume that all the monitored variables are encoded by using 16 bits. Table 2.

Table 2 – List of key sensors and corresponding parameters

Variable	Sensor	Time constant (s)	Signal Range	Variable Range	# bits
Control Rod Position	Linear transducer	-	-	-	16
Cold Leg Temperature	TC (K-type)	3	0-78 mV	0-1250 °C	16
Core Exit Temperature	TC	3	0-78 mV	0-1250 °C	16
RCS Pressure	Strain pressure transducer	0.25	0-20 mA	0-500 Pa	16
RCS Inventory	Differential pressure transducer	<1	0-20 mA	0-500 Pa	16
Containment Sump Water Level	Differential pressure transducer	<1	0-20 mA	0-500 Pa	16
Containment Pressure	Strain pressure transducer	0.25	0-20 mA	0-500 Pa	16
Containment Isolation Valve Position	Potentiometer	<1	0-5 V	0-359°	16
Hydrogen Concentration	Electrochemical Galvanic cell	30	-	-	16
SG level	Differential pressure transducer	<1	0-20 mA	0-500 Pa	16
SG pressure	Strain pressure transducer	0.25	0-20 mA	0-500 Pa	16

Comments below provide a slightly expanded discussion of the parameters of a few select process variables and corresponding measurement sensors:

2.2.1. Cold leg temperature

PWR plants often employ 20 to 40 RTDs to measure the fluid temperature in the reactor coolant system. RTDs are used in PWR plants to measure the primary coolant temperature. Typically, these RTDs are installed in thermowells that are welded to the primary coolant piping. The temperatures measured by the RTDs are used by the plant operators for process control and to assess the operational status and safety of the plant.

2.2.2. Core exit temperature

In addition to the RTDs, there are also about 50 core-exit thermocouples (CETs) in PWRs to provide an additional way to monitor reactor coolant temperature. Accuracy for CETs is not as important as for RTDs because CETs are used mostly for temperature monitoring. In each loop of a PWR plant and for each core quadrant, redundant RTDs and CETs are used to minimize the probability of failure of any one RTD or CET affecting the safety of the plant.

2.2.3. Hydrogen concentration

The concentration of hydrogen within the containment is assumed to be measured by using a palladium-based thick film sensor. The characteristic response times are equal to 20-30 seconds, and the recovery times are of the same magnitude. This slow dynamics is due to the long time constants associated with the diffusion of hydrogen into the palladium layer, and the effects of temperature.

2.3 Data transmission and power consumption

Figure 1 provides conceptual visualization of data transmission rates. In particular, the upper theoretical bound (*Channel Capacity (Shannon Limit)*) is derived from the information theory, Eq. (1).

$$C = W log_2 \left(1 + \frac{P}{N_0 W}\right) \tag{1}$$

The limits imposed by the data collection rates due to the sensor features (*Sensor dynamics-limited Channel Capabilities*) are more penalizing. Finally, the minimum data rate is the one which allows meeting the minimum monitoring level imposed by the unit safety (*Safety-oriented Performance*). As previously mentioned, during post-accident scenarios, the system evolution is pretty slow, and we are not expecting the system conditions to abruptly vary. As first tentative guess, we might assume that the system conditions might be updated every minute. This value can be considered as the lower acceptable bound for the data transmission rate for safety-grade monitoring purposes.

$$\tau_{safety} = 1 \text{ min} \tag{2}$$

$$f^{min} = f_{safety} = \frac{1}{\tau_{safety}} \tag{3}$$

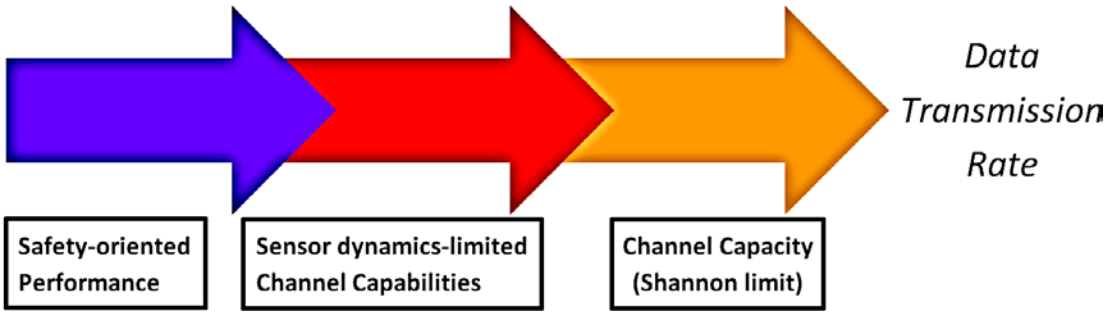

Figure 2 – Visualization of data transmission requirements.

In development of preliminary data transmission protocols, the following assumptions have been made:

(1) Train of signals, i.e. the sensor outputs are progressively collected and then transmitted at the same time.
(2) The number of bits dedicated to encode the instantaneous value of a certain variable is constant.
(3) As first guess, 16 bits are assumed to be used for all the monitored variables.
(4) PSK communication protocol, i.e. constant power consumption to encode zeros and ones.

Accordingly, the overall length of the transmitted binary string (L) is equal to the sum of the number of bits you need to encode each one of the M monitored variables together with the 4-digits Barker sequence, Eq. (4).

$$L(t) = L = 4 + \sum_{j=1}^{M} N_j \qquad \text{where } j = 1,2, \dots, M \tag{4}$$

In virtue of assumption (2), the length of the train of signals is always the same. In order to evaluate the energy consumption for every train of signals, the first step is the definition of the number of bits dedicated to encode the variables listed in Table 2. In virtue of assumption (2), we will assume 16 bits for all the monitored variables. Therefore,

$$L(t) = L = 196 \text{ bits} \tag{5}$$

The main consequence of the adoption of the PSK communication protocol (assumption (4)) is that the energy consumption to encode a logic ″1″ or ″0″ ($e^{1,0}$) is the same. Therefore, the

energy consumption for the transmission of each one of the M variables ($e(j)$) only depends on the number of dedicated bits ($\#bit(j)$).

$$e(j) = e^{1,0} \cdot \#bit(j) \tag{6}$$

Consequently, every train of signals consumes the same amount of energy. This result tremendously simplifies the problem, since the stochastic nature of power consumption is removed, and more accurate estimates of the sampling frequency bounds according to the power consumption criterion can be derived. As a first guess (assumption (3)), we will have

$$e_{TRAIN}(t) = e_{TRAIN} \cong e^{1,0} \cdot 196 \tag{7}$$

As for the single digit power consumption, the bit pulse is characterized by a minimal length value. In particular, if a pulse is shorter than $100\ \mu s$, it is difficult to determine if it is $''1''$ or $''0''$

The proposed approach is based on the collection of all the sensor output signals, which are eventually transmitted at the same time as a train of signals. The sensors listed in Table 2 are characterized by very different time constants. According to the proposed approach, the frequency of transmission (f) is set equal to the reciprocal of the time constant of the slowest dynamics sensor (τ_M), i.e. 30 seconds. Unfortunately, this frequency might be too low. Therefore, an alternative communication approach, illustrated in Figure 3, could be utilized. Let us set the frequency of transmission equal to the time constant of the second slowest dynamics sensor (τ_{M-1}), which is expected to be much lower than 30 seconds. In this way, when the collected measurement outcomes are transmitted, the measurement of the hydrogen concentration will not be complete, and then the previously obtained value will be used. This scheme is not efficient. Therefore, in the proposed approach, the hydrogen conditions will be transmitted only when the measurements have been completed; when they have not, a shorter train signals will be transmitted.

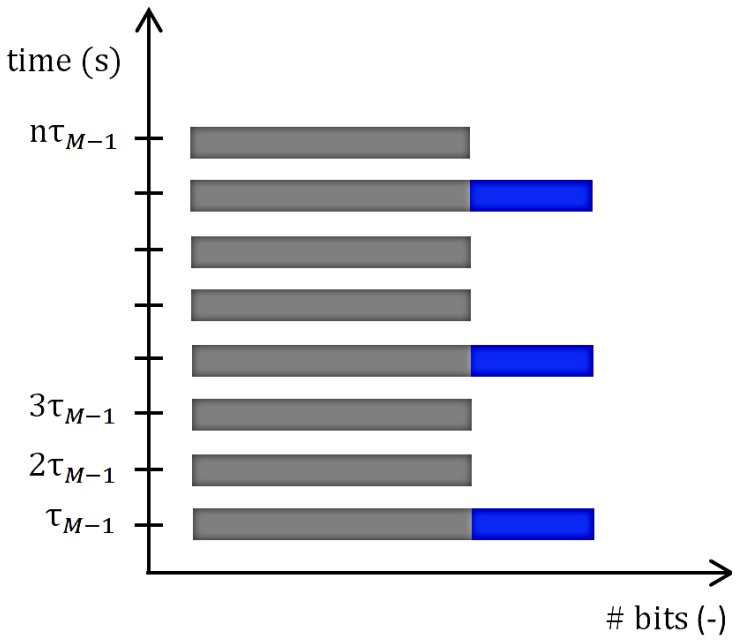

Figure 3 – Alternative transmission scheme.

Let us assume that the transmission frequency is equal to f. Then, the time can be discretized in $\left(\frac{1}{f}\right)$-long time periods. Each time period is composed by two phases, i.e. the signal collection and the signal transmission, as shown in Figure 4.

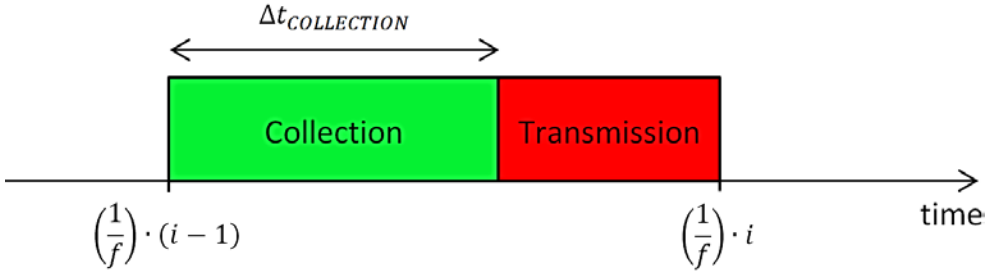

Figure 4 – Collection-transmission scheme.

The evaluation of the energy consumed in every time period (e) strongly affects the value of the maximum transmission frequency which is compatible with the battery pack energy availability, Eq. (8).

$$f^{max} = \left(\frac{100\ kWh}{72h}\right) \cdot \frac{1}{e} \tag{8}$$

The time period energy consumption is given by the sum of the Red Pitaya-related energy consumption during the signal collection phase and the energy consumed to transmit the train of signals, Eq. (9). In this regard, the Red Pitaya-related energy consumption is assumed to be uniform during the signal collection phase, whose duration is equal to $\Delta t_{COLLECTION}$.

$$e = \text{Power}(RedPitaya) \cdot \Delta t_{COLLECTION} + e_{TRAIN} \quad (9)$$

To compare the PZT with the EMAT configuration, the corresponding energy consumption needs to be evaluated. Once we derived that, the corresponding maximum transmission frequency compatible with the battery back availability criterion (f^{max}) needs to be derived, i.e. the power consumption needs to be such that the system conditions can be continuously monitored for 72 hours. At this point, if f^{max} is lower than f_{safety}, the corresponding technology cannot be adopted, Eq. (10).

$$f^{max} \geq f_{safety} \quad (10)$$

In particular, if the considered technology-related energy consumption (e_{EMAT} and e_{PZT}) is such that the maximum frequency which allows monitoring the system for 72 hours is lower than f_{safety}, it means that the energy consumption is too high and it does not allow to get system updated every minute, and then the technology is not suitable for this purpose.

3. Acoustic Communication Channel Design

Using the communication protocol described in Section 2, we have demonstrated data transmission over a communication channel consisting of two PZT's on six-foot long stainless steel pipe. As described in previous reports, the parameters of the pipe in this study closely resembles those of the chemical volume control system (CVCS) charging line pipe, which penetrates through the containment building wall in some common reactor designs.

3.1. Acoustic transducer frequency selection

As discussed in Section 1, higher frequency of the carrier acoustic wave allows for transmitting information at high bit rate. As illustrated below, information is encoded with D/A into a square wave waveform with duty cycle. As an example, time-domain waveform with duty cycle of 100μs and its spectrum calculated with FFT are shown in Figure 5.

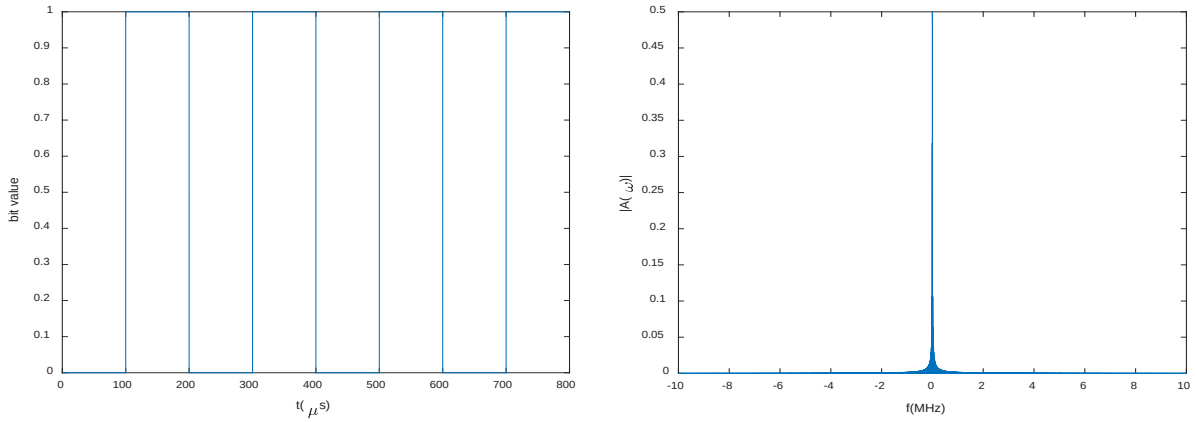

Figure 5 – Information-carrying waveform (left) time domain (right) frequency domain

The waveform is encoded as amplitude modulation of the carrier with acoustic frequency. Figure 6 shows amplitude modulated 2MHz carrier frequency and its FFT spectrum.

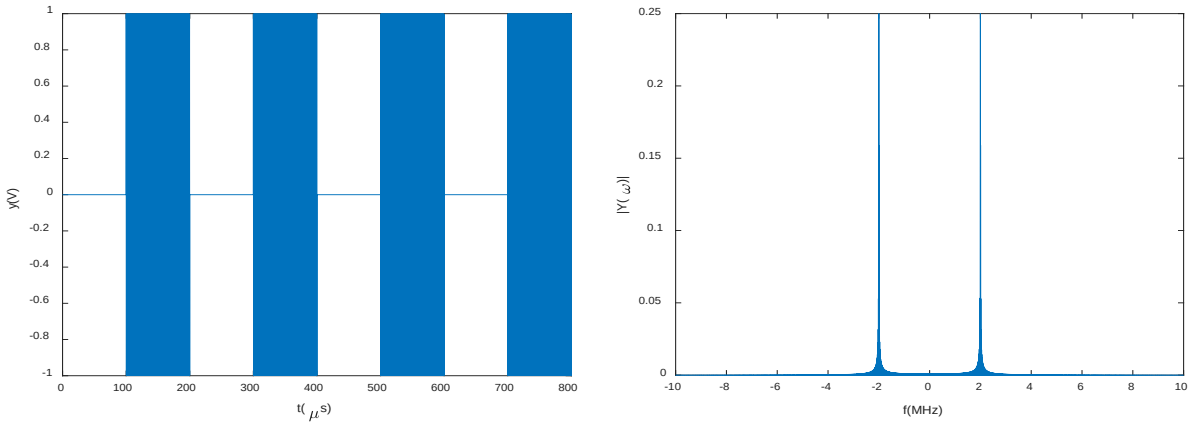

Figure 6 – Amplitude-modulated carrier waveform (left) time domain (right) frequency domain

Demodulation at the receiver occurs by multiplying received signal by a reference sinusoid with the same acoustic frequency. The signal after multiplication and its FFT spectrum are shown in Figure 7.

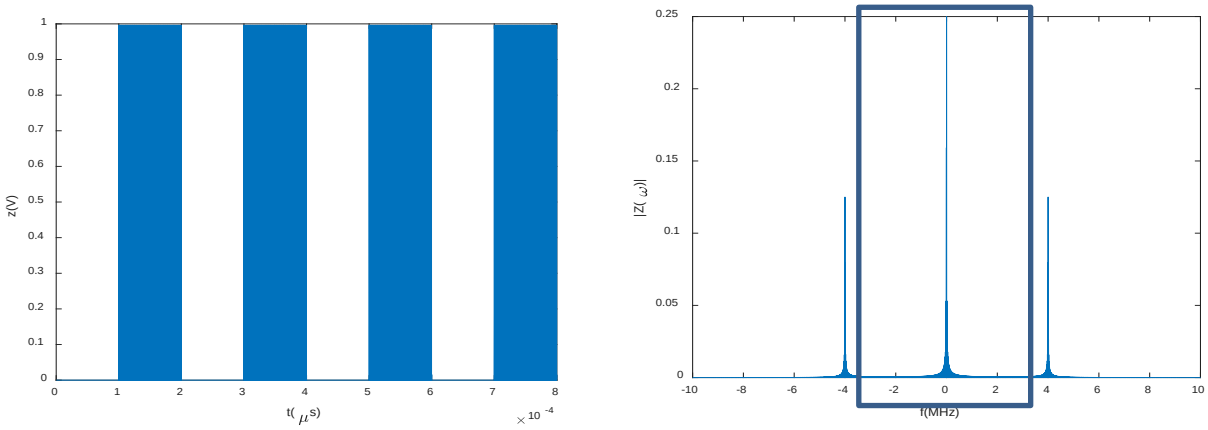

Figure 7 – Received signal multiplied by reference (left) time domain (right) frequency domain

Demodulation takes place by applying low-pass filter (LPF), shown as the box in the spectral plot, to remove carrier sidebands at 2f = 4MHz. The spectrum of information-carrying square wave is close to DC. For higher-frequency amplitude modulation (AM) square wave, the baseband spectrum will increase. The spectral width of the LPF or the frequency of the carrier will determine the limit of AM duty cycle. Thus information bit rate is proportional to frequency of the carrier f.

At the same time, higher frequency results in larger absorption losses in the channel. A decrease in the plane harmonic wave amplitude as a result of its interaction with a medium takes place according to the Beer-Lambert law $e^{-\delta x}$, where x is the distance that the wave passes in the medium and δ is the damping coefficient. In what follows, the term "damping" will refer only to the wave amplitude decrease that is considered by an exponential multiplier, contrary to a decrease in the amplitude related to the wave front extension.

The damping factor consists of the coefficients of absorption δ_1 and dissipation δ_2: $\delta = \delta_1 + \delta_2$. During absorption, a sound energy transforms to thermal, and during dissipation the energy remains sonic, but is emitted by a wave whose propagation is directional. Absorption is conditioned by ductility, elastic hysteresis (i.e., by a different elastic dependence during extension and compression), and heat conductivity.

The value of the dispersion coefficient in a medium is greatly affected by the correlation of the average size of heterogeneities and the average distance between heterogeneities with the elastic wavelength. In metals, the medium parameter that significantly affects the dispersion of crystals is the average size of a particle $\tilde{d}$. Then, total damping of stainless steel is calculated by the equation

$$\delta = Af + Bf^4\tilde{d} \qquad (11)$$

Where A and B is the constant. The average size $\tilde{d}$ of stainless steel is 1.5μm. Thus, the quadratic frequency term can be ignored, and attenuation in the channel is linearly proportional carrier frequency.

Commercially available PZT's are built for operation at a set of discrete frequency. In this study, considering tradeoffs between bit rate and attenuation, we have chosen PZT operating at 2MHz. Losses incurred due to attenuation in the channel were compensated with power amplifier (transmitter side) and low-noise amplifiers (receiver side).

3.2 Wedge selection for PZT refracted shear wave

Computer simulations were performed with COMSOL Multiphysics™ software package to provide support to ongoing experimental efforts described in previous reports (Heifetz 2017, Heifetz 2018). The objective of computer simulations described in this report is to develop better understanding of loss terms associated with coupling and propagation of elastic waves in the piping structure communication link. In prior work, we have modeled propagation of elastic waves generated on a pipe with a radially symmetric collar-type transducer (Bakhtiari 2017). However, we have subsequently determined that most likely conduits of elastic waves for information transmission out of the containment building are stainless steel pipes of the chemical volume and control system (CVCS) charging line (Heifetz 2017). These pipes are part of the thermal hydraulic system, and as such are enclosed by a layer of thermal insulation. Thermal insulation materials, such as mineral wool, are poor transmitters of acoustic waves. To achieve efficient coupling of acoustic waves into the pipe, the insulation material has to be removed for transducer to be directly in contact with the metal pipe. Thus, it is preferable to use a transducer with the smallest form factor so that minimal amount of thermal insulation needs to be removed and no thermal imbalances in the coolant system are created.

In this study, we have modeled propagation of refracted shear wave coupled into stainless steel pipe with an angled wedge. Such arrangement has a smaller form and requires removal of smaller amount of thermal insulation, as compared to ring of transducer. Two-dimensional simulations were developed to analyze propagation of elastic waves in the axial direction of the pipe, as well as in the radial cross section of the pipe. A three-dimensional simulation combined these results to visualize propagating both radially and axially around the pipe. The 3-D simulations indicate that the refracted shear waves on a pipe are created in a torsional mode

3.2.1. Computational model setup

Software package COMSOL Multiphysics™ was used to model elastic waves propagating on a steel pipe structure for 2-D and 3-D computational model cases. Computer simulations of the general setup shown in Figure 8 were performed using the Solid Mechanics Module of COMSOL. The acoustic wave transducer was modeled as a PZT device. Although COMSOL library contains a module simulating PZT performance, we have determined through simulations that using the library module is computationally expensive. Instead, in this project we developed a computationally efficient model of a source of longitudinal acoustic waves. In this model, acoustic waves were generated with a rectangular iron block vibrating at an ultrasonic frequency against a

plastic wedge. The amplitude of displacement of the iron block is on the order of a micrometer. In this study, unless stated otherwise, the default value of the ultrasonic frequency is 500 kHz. Note that vibration plane of the iron block was oriented at the same angle as that of the wedge incline. To match the experiment, the material for wedge and pipe in the COMSOL model were selected to be acrylic and steel, respectively. The ambient medium in the computational grid was chosen to be vacuum. The receiver acoustic transducer (shown with dashed lines in Figure 8) was not explicitly modeled in our computer simulations. Instead, elastic wave pressure and displacement values were obtained directly from the computational grid at observation points along the pipe.

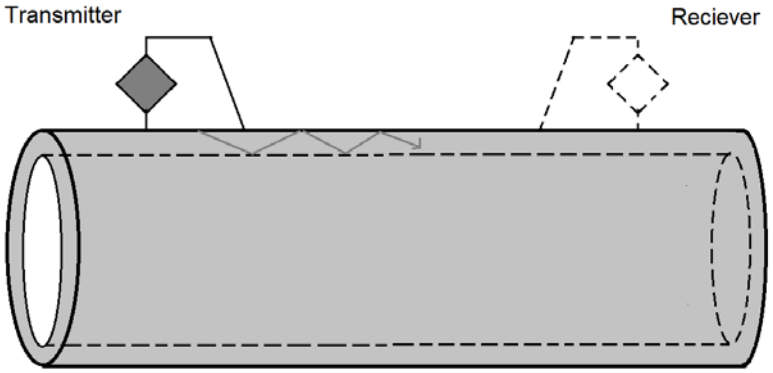

Figure 8 – Pipe-transducer model setup for computer simulation. Transducer sizes and angles are drawn not to scale. The receiver transducer (indicated with dashed lines) was not explicitly modelled in this study.

Three different approaches were pursued to model refracted shear elastic wave propagation on the piping structure. First, a two-dimensional model of radial cross section of the pipe was studied to determine radial wave propagation on the pipe. Second, a two-dimensional of refracted acoustic wave with angled beam into a steel plate was considered to investigate axial propagation of elastic waves the pipe. Finally, in the third approach, simulations for a complete three-dimensional wedge/pipe model were performed.

3.2.2. Two-Dimensional Radial Cross-Section Simulations

Elastic wave propagation on radial cross-section of a pipe was investigated for contoured wedges with different surfaces. The objective of this study was to determine how the contact area between dielectric wedge and metallic pipe affects the amplitude of elastic wave coupled into the pipe. Three different wedge contact areas were studied, as shown with color-coded combinations in Figure 9. The distance from the top of the pipe to the bottom of transducer (gray box) was held constant at 10mm for all wedges. The radius of the pipe was set to 3.5cm to match the experiment, The wedge with minimal contact area (black box) only had the wedge and the pipe connecting along the line at the top of the pipe. The partial contact wedge (black and red) had a contoured surface, enclosing a portion of the top arch of the pipe, with straight flanges on both sides. The

total contact wedge (black, red and blue) had the entire width of the wedge contoured to match the pipe radius, and thus provided the largest contact surface area with the pipe.

Acoustic wave amplitude measured as total displacement for the three types of wedges in Figure 9 are displayed in Figure 10 The displacement obtained with each wedge in Figure 3 is plotted at different times as function of pipe circular cross-section polar angle. The top of the pipe corresponds to 90^o polar angle in these plots. Results are presented for 500 KHz frequency. Similar patterns were observed for different frequencies. To follow time evolution of the elastic wave propagation in the structure, waves coupling into the pipe reflects off the inner surface of the pipe. For waves at normal incidence, propagation would consist of bouncing between the top and bottom surfaces of the pipe. However, most of signal wave front are incident at an angle to the vertical, Reflections at the inner pipe surface are causing the waves to propagate around the pipe in both the clockwise and counterclockwise directions. Once both of these signals reach the bottom of the pipe at 270^o angle in Figure 4, they begin to interfere with each other, thus potentially creating noise in the communication system.

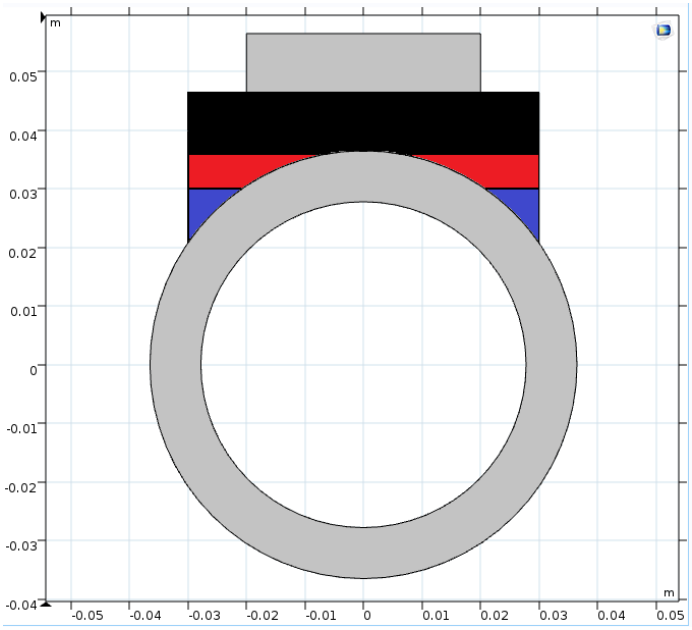

Figure 9 – Wave propagation along radial cross section of the pipe. The distance between the bottom of the transducer (gray box) and the top point of the pipe is 10 mm. Different contact area contoured wedges are indicated with different combination of colors: Line contact (black), partial connection (black & red), and full connection (black, red & blue).

When different contact surface wedges were examined in Figure 10, it was concluded that as contact between the pipe and the wedge is limited, a clearer signal emerges. This result appears as a byproduct of limiting the signal's angular span of coupling into the pipe, and thus limiting the amount of reflections in the shell of the pipe. Without many reflections from the inner surface, there is less angular spread of the signal into the pipe, which could lead to a pattern of constructive

and destructive interferences. However, by limiting the angular spread of the coupled beam, the total power of the acoustic signal coupled into the pipe is reduced as well.

These results suggest a trade-off between signal intensity and communication signal noise. The conclusion is that the optimal wedge is the one with partial contact (black & red colors in Figure 9), where enough power is given to the signal to reach the end of the pipe, but at the same time no strong interferences are generated to create bit errors.

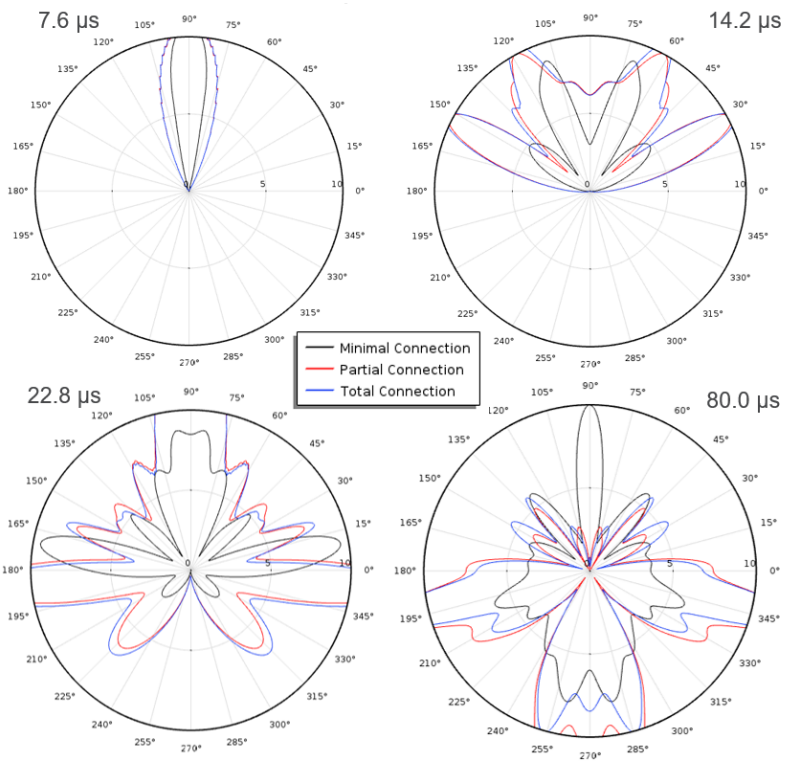

Figure 10 – Acoustic wave amplitude measured as displacement on pipe surface. The displacement obtained with each wedge in Figure 3 is plotted at different times as function of pipe circular cross-section polar angle. Results are presented for 500 KHz frequency. Similar patterns were observed for different frequencies.

3.2.3. Two-Dimensional Axial Cross-Section Simulations

In the axial cross-section wave propagation study, wave propagation only over the top part of the pipe in contact with the transducer were considered. Thus, the cross-section of the pipe was represented by a plate with the same thickness as cylindrical shell (8.7mm to match experiment). Results of computer simulations showing acoustic wave intensity profile measured as pressure distribution after 100µs from the start of acoustic wave transmission are shown in Figure 11. The five panels in Figure 11 show radial acoustic wave intensity distribution for 500KHz, 1MHz, 1.5MHz, 2MHz, and 2.5MHz frequencies. We have observed that for some frequencies, the power of the signal coupled into the pipe was a significantly lower than that of other frequencies. Qualitatively similar phenomena has been previously observed in experiments as well (Heifetz

2017). To investigate this further, multiple scattering within the wedge was studied. Within the wedge, a significant amount of the signal was reflected back from the plastic - steel boundary because of high impedance mismatch. This signal, despite the non-reflecting boundary condition on the outer walls of the wedge, reverberated continuously within the wedge. When these reflections compounded, a significant amount of scattering inside the wedge was created at higher frequencies. This is shown by comparison of acoustic pressure distribution inside the wedges at 500KHz and 2.5MHz in Figure 12. In some cases, such as 1 MHz and 2 MHz, this caused a large amount of destructive interference. We believed this destructive interference attributed to some on the frequency disappearance seen in Fig. 10. We found for lower frequencies, such as 500 kHz, these reflections die out faster, as seen in Figure 12a, causing less disruption of the signal. It is unclear if the reflections within the wedge itself are a product of the simulation or are actual present in the system itself. Reflections within the wedge could be potentially suppressed by optimizing the angle with which the waves are incident at the plastic-steel boundary.

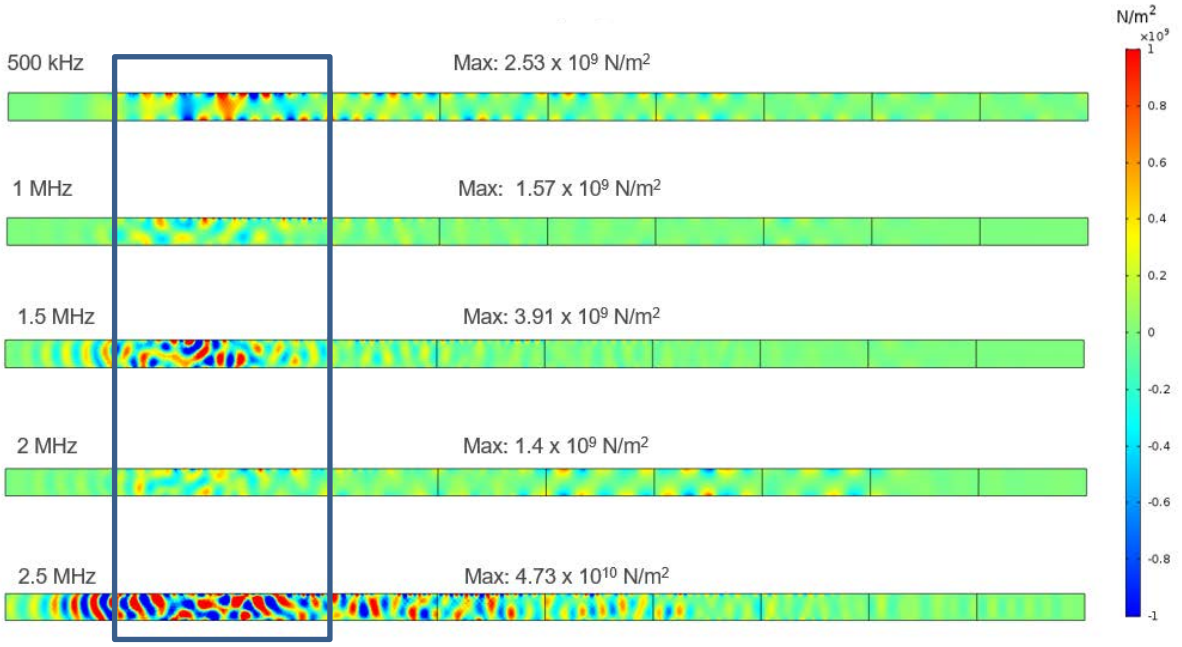

Figure 11 – Acoustic wave intensity profile measured as pressure distribution in the axial direction after 100μs of signal transmission. The wedge position is indicated with an overlaying box.

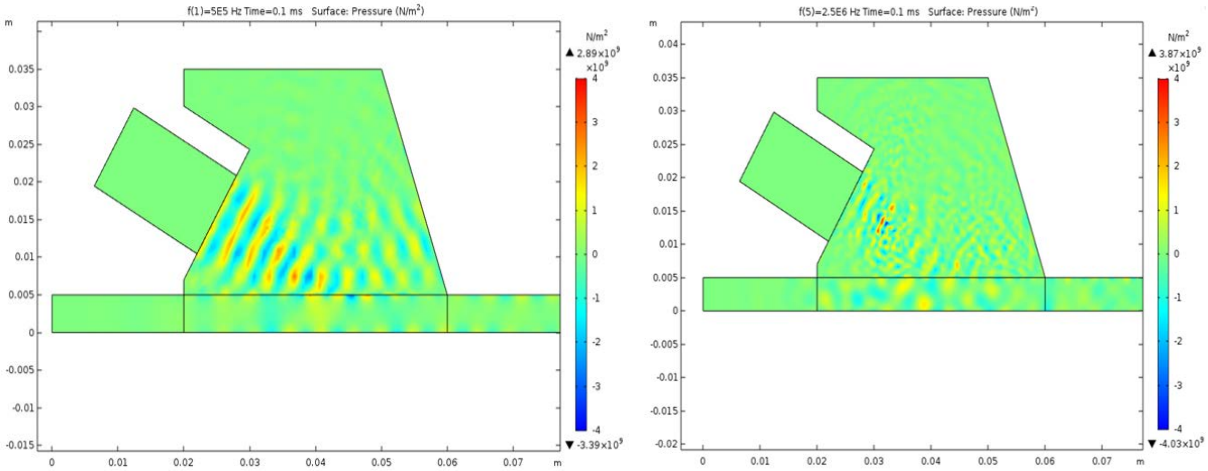

(a) **(b)**

Figure 12 – Multiple reflections of acoustic wave inside the wedge for (a) 500 kHz and (b) 2.5 MHz transducer frequency.

3.2.5. Three-Dimensional Simulations

Three dimensional simulations were performed to model wave propagation in a section of a steel pipe of length 12.5 m, radius of 3.5 cm and thickness of 8.7 mm. The transducer was modeled as PZT represented by an iron block vibrating perpendicular to the acrylic plastic wedge surface at 500 kHz. This amplitude of displacement of the iron block was on the order of a micrometer. The wedge was assumed to be in partial contact with the pipe, as shown in Figure 9. Results of 3-D simulations which visualize distribution of elastic wave intensity are shown in Figure 13. The elastic wave intensity distributions resulting from coupling with 30^o and 45^o angled wedges are shown in Figures 13(a) and 13(b), respectively. These results indicate that 3-D propagation of elastic wave occurs in angular and axial directions, in agreement with 2-D simulations. The simulations indicate that refracted shear waves are excited in a torsional mode on the pipe, with rotations in both clockwise and counterclockwise directions. Because we were able to simulate only a small section of the pipe due to computer memory limitations, we could not visualize far field of the acoustic wave. These findings agree qualitatively with experiments which indicate that a signal could be received across the pipe when receiving PZT is positioned at 90^o and 180^o relative to the transmitting PZT. This indicates that the communication system is resilient to misalignment of transducers.

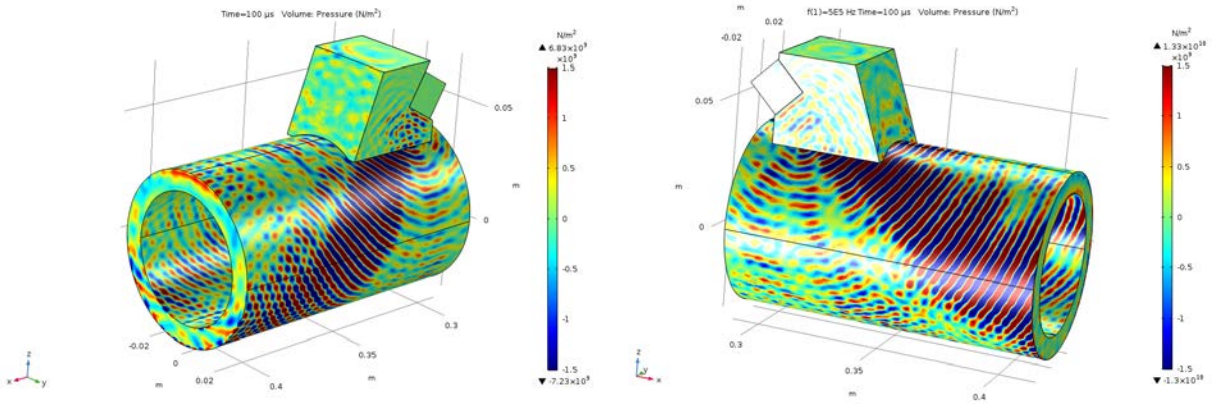

(a) **(b)**

Figure 13 – Three dimensional simulation indicate torsional modes of the refracted shear wave on the pipe for excitation with (a) 30º angle wedge and (b) 45º angle wedge.

3.2.6. Experimental Validation

As described in Section 1, physical realization of communication channel with PZT requires generation of single mode wave. This can be accomplished via generating a refracted shear wave with PZT mounted on angled wedge. Commercially available plastic wedges have 30º, 45º and 60º angles of incline. The first critical angle for plastic to stainless steel interface is approximately 29.5º, so that, in principle both 30º, 45º wedges are suitable. However, we have observed experimentally that using contoured 30º wedge results in generating in both longitudinal and shear waves in the pipe. The modes were inferred from calculated velocities of pulses (5790m/s and 3100m/s for longitudinal and shear wave velocities in stainless steel, respectively). Generation of longitudinal modes was possibly an artifact of relatively small radius of curvature of the pipe, such that parts of the wavefront were actually incident at the interface at angles smaller than the critical angle.

When using a 45º wedge without contouring, we have observed that only shear waves were generated in the pipe. At the same time, the amplitude of the refracted shear wave was slightly smaller than that of generated with a contoured wedge. This is consistent with prior findings indicating that larger surface area of contact between wedge and pipe are results in better coupling of elastic wave energy into the pipe at the expense of reducing signal clarity.

For verification that only shear wave is generated, signals were measured on a stainless steel plate and stainless steel pipe of similar thicknesses. The same set of wedges and transducers separated by the same distances were used for plate and pipe measurements. Figure 14 displays the schematics of the experimental arrangement. A pair of 2MHz PZT transducers separated by a distance of 165cm was used in this study. Transmitted pulses were of 200μs time duration.

Comparison of time-domain signals transmitted on a plate and on a pipe are shown in Figure 15. Signal transmitted on a plate is shown in Figure 15(a), while those for transmission on a pipe are shown in Figures 15(b), (c) and (d). To validate COMSOL computer simulations predicting excitation of torsional waves on a pipe, receiver and transmitter at the ends of the pipe were aligned

(Figure 15b), rotated by relative 90^{o} angle (Figure 15c), and rotated by relative 180^{o} angle (Figure 15d). The signal velocity obtained in all cases on plate and pipe was close to 3100m/s value, confirming that only shear wave modes were present in the channel. In addition, it appears that transmission is nearly insensitive to the relative angle between transmitter and receiver transducers, which confirms prediction of torsional wave excitation on a pipe. Insensitivity to alignment between transmitter and receiver is advantageous for communication system robustness, since exact alignment would be difficult to perform in field conditions at a nuclear power plant.

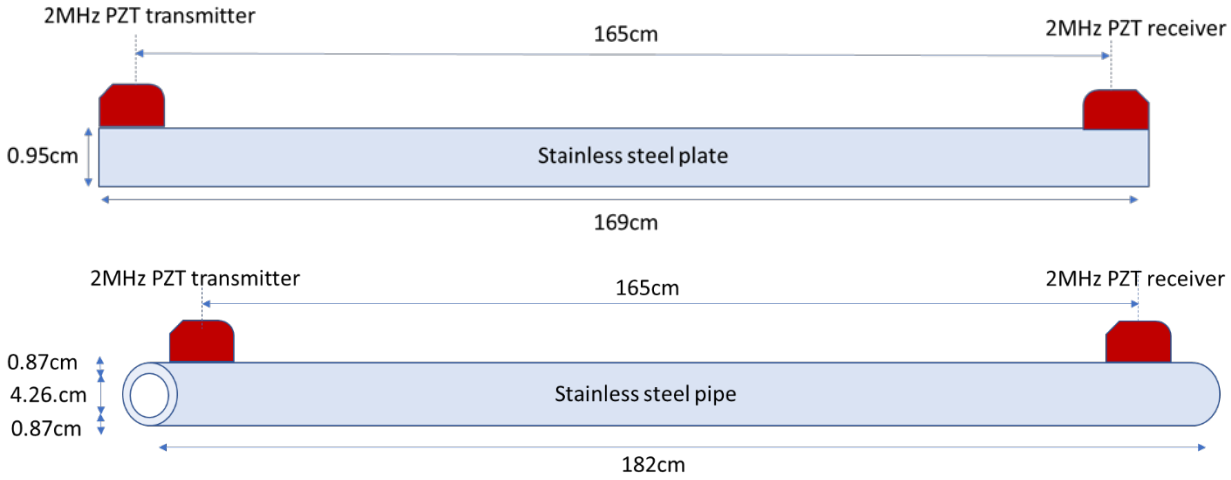

Figure 14 – Communication channels based refracted shear waves in stainless steel with PZT's on 45^{o} angled wedge. The channels are stainless steel plate (top) and pipe (bottom)

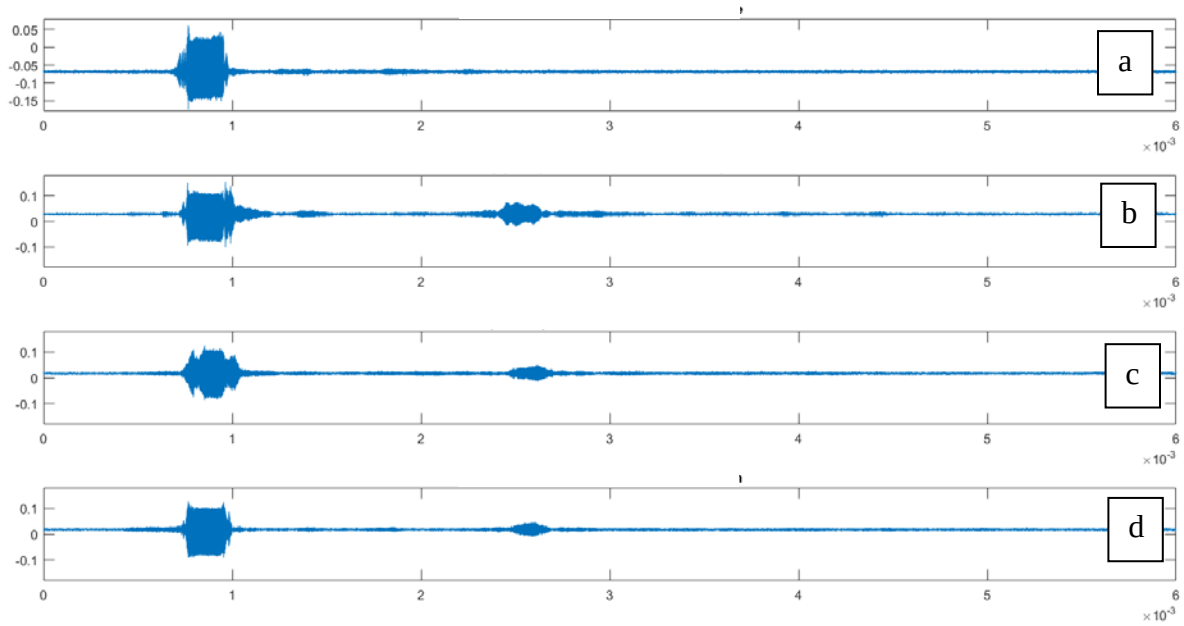

Figure 15 – Time domain signals on plate and pipe: (a) transmission on plate, (b) transmission on pipe with transmitter and receiver aligned, (c) transmission on pipe with

receiver and transmitter rotated by relative 90º, (d) transmission on a pipe with transmitter and receiver rotated by relative 180º

3.3 Resilience of Communication System to Interferences

Proof-of-principle studies were conducted to investigate performance of communication system under laboratory conditions designed to introduce some interferences to elastic wave propagation on a pipe, which are representative of actual deployment scenario.

3.3.1. Effect of Supporting Baffle Plates on Transmission

As outlined in previous reports on this project, the candidate pipe for acoustic communication across containment building wall is a charging line of CVCS. This pipe penetrates through a special sealed tunnel in the containment building wall. The pipe is welded to baffle plates, which are bolted to interior and exterior surfaces of the containment wall, thus sealing the tunnel (Figure 16a). In this project, we designed and fabricated stainless steel baffle plates to anchor pipe to optical bench to simulate mechanical constraints at actual NPP (Figure 16b).

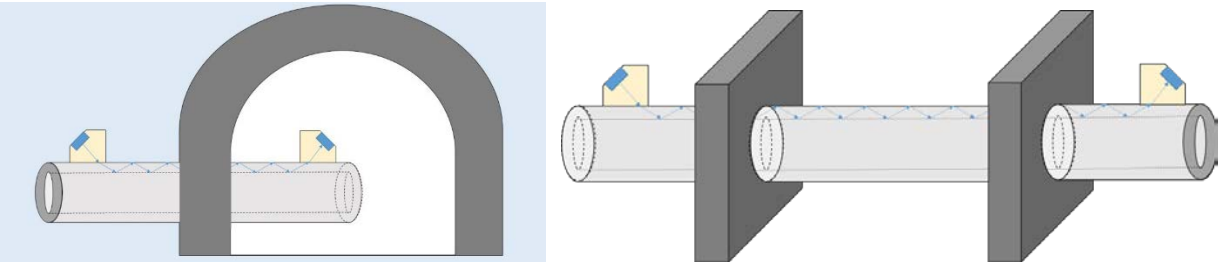

(a) (b)

Figure 16 – (a) Envisioned deployment at NPP. (b) Laboratory bench scale setup of pipe with supporting baffle plates.

Dimensions of the stainless steel baffle plates are shown in Figure 17. Each plate was made out of two pieces, with semicircular cutout designed to fit to the pipe. Through holes for ¼-20 screws were made for assembly of the entire construction on an optical bench. When assembled, baffle plates provided support to the pipe.

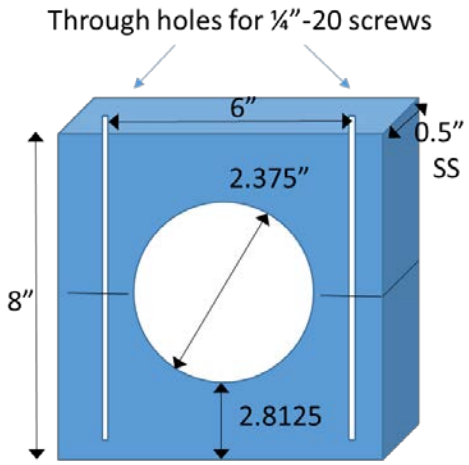

Figure 17 – Design and dimensions of each baffle plate.

To study the effect of signal attenuation due to baffle plates, refracted shear wave signal was transmitted over the length of the pipe (1.65m), with PZT transducers positions outside the baffle plate as shown in Figure 16b. For comparison, the pipe on rested on two small cardboard boxes, and Comparison of the two signals showed slight attenuation of the acoustic signal due to baffle plates. This is to be expected, since baffle plates provide a radial support to the pipe, and little coupling of shear waves from the pipe is expected to radially attached structures.

3.3.2. Effect of Coupled Low Frequency Process Noise on Signal Transmission

Process noises due to operating machinery at a nuclear facility can potentially couple to the pipe and interfere with AC system. These noises tend be primary audible low-frequency ones, with typical bandwidth below 10KHz.We have devised a study to investigate resilience of ultrasonic data transmission over pipe to low frequency noise. Process noise was experimentally simulated with frequency-tunable mechanical shaker placed in contact with pipe to induce low-frequency vibrations in the pipe. The photograph of the setup is shown in Figure 18.

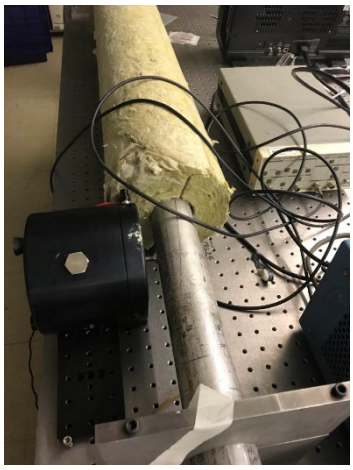

Figure 18 – Frequency-tunable mechanical shaker in contact with pipe.

Transmitted OOK acoustic digital signals with 200μs bit duration at 2MHz shear wave carrier are shown in Figure 19. The reference acoustic signal received with mechanical shaker turned off is shown in Figure 19(a). Received acoustic signals with the pipe vibrated at 100Hz, 1KHz, 10KHz are shown in Figure 19(b), 19(c) and 19(d), respectively. No significant changes in the transmitted signal caused by pipe vibration could be observed. Results of this study suggest that low-frequency process noise produces negligible interference effect on ultrasonic 2MHz shear wave information-carrying signal.

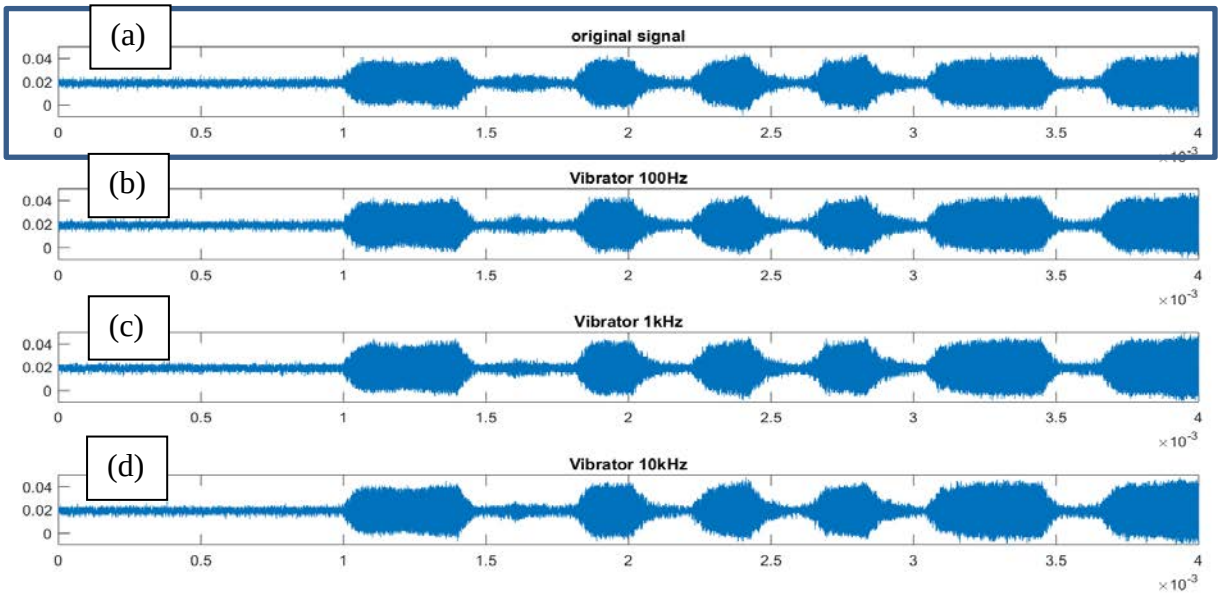

Figure 19 – Effect of mechanical vibrations on ultrasonic signal. Received acoustic signal has 2MHz carrier frequency and 200μs bit pulse duration. (a) Received signal on a pipe with no vibration. (b) Received signal on pipe vibrated at 100Hz (c) Received signal on pipe vibrated at 1KHz. (d) Received signal on pipe vibrated at 10KHz.

3.4 Preliminary Evaluation of Data Transmission with EMAT-based Channel

3.4.1. Transmission and reception of EMAT-generated signal

Shear-Horizontal (SH) wave is one of the plate waves which is well suited for ultrasonic communication. Advantages of SH wave is that they are not attenuated by water and less attenuated by the coating of the solids and it suffer little energy loss when propagate in the solids. If SH wave is obliquely incident on a free surface, there will be no mode conversion from SH wave to longitudinal wave or SV (shear vertical wave). Which means that the received signal is easy to analysis the multipath effect of the channel, as there is one certain type of SH wave modes exist. Generally, SH wave is generated by angle beam piezoelectric transducer and may suffer from the ambiguity in signal quality due to uncertainty in a coupling condition. However, an EMAT can selectively excite different kinds of SH waves requiring no direct contact with the samples. In addition, EMAT holds promise for ultrasonic signal generation in harsh environment (high temperature, radiation).

Since communication channel has finite length and EMAT transducer generate (receiver) signals in forward direction and backward direction, more reflections can be seen in the receiver side compared with PZT transducer. An experiment is setup to show the interference and reflection. The schematics of EMAT-based communication channel on a stainless-steel plate are shown in Figure 20. In order to see the see better reflection, the transmitter and receiver is set 30cm from the edge.

Figure 20 – Schematics of EMAT-based communication channel on a plate

A 100μs bit duration pulse is sent by transmitter, and Figure 34 shows the signal picked up by the receiver. We can see that the amplitude of signals of different frequencies and matches with frequency response. The reflections from Group 1 are directly from 2 edges of steel plate and reflections from Group 2 are signals which next round reflection. SH waves are selected with different frequencies and they travel in different velocities. Group 1 signal travel 2 times long of steel plate arrives at Group 2. All these reflections will affect communication efficiency and bit error rate. We can see the attenuation is proportional frequency. It means that the lower frequency ultrasonic signal like 230kHz can propagation longer. However, the attenuation can restrain the Group 2 and later reflection signals. In this channel, we set transmitter and receiver next to the edge which can remove part of the group 1 reflection and set a longer bit duration to make the reflections overlap. Considering the power efficiency and less Group 2 reflection, we will choose around 400kHz as the carrier frequency.

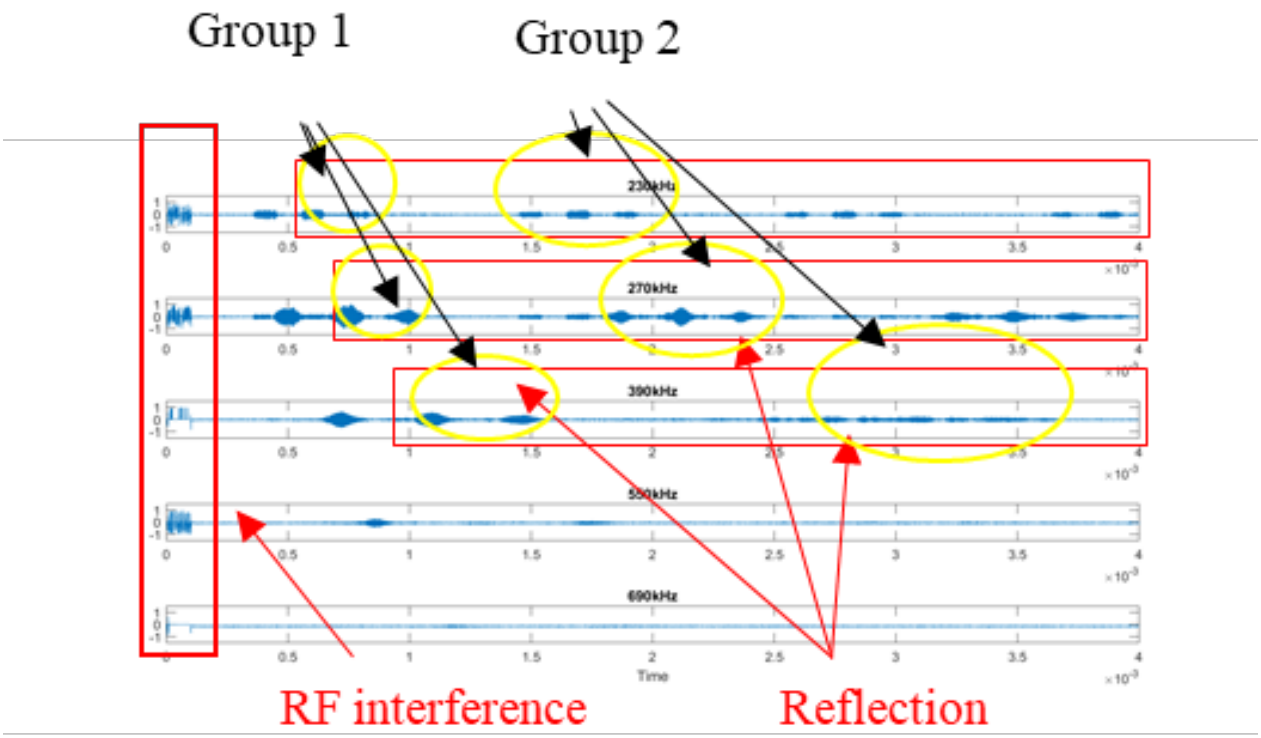

Figure 21 – Signal reflections and interferences in EMAT-based channel

EMAT transmitter needs a large power excitation to generate ultrasonic signal. Any imbalance in the communication system cause the BNC cable, power wires and every other interconnection to become part of the transmitter and radiate. the interference can be seen in Figure 21 is at least 5 times larger than the ultrasonic signal. If the interference is not removed, the system can't communicate with ultrasonic signal. As a result, an impedance matching network is implemented in receiver side to improve the quality of received signal and isolated the RF interference.

3.4.2. Efficiency of acoustic signal transduction

Transduction efficiency between electric energy and sound energy with an EMAT is much lower than PZT. For the transmitter side, the impedance of EMAT is similar to the power amplifier. In the receiver side, there is large impedance mismatch between EMAT receiver (140 Ωresistive) and low-noise amplifier (100MΩ resistive), which will cause inefficient transfer the acoustic wave into electric energy. An INNERSPEC signal conditioning box (SCB) is implemented as the impedance matching. There is ground connector on the SCB and additional ground path is added for the receiver. Meanwhile, the steel plate channel has to be grounded. The interference is highly restrained and will not affect the ultrasonic communication.

Further work is aimed at developing custom EMAT's to increase amplitude of coupled signal. Figure 22 shows the commercial EMAT with an array of magnets in flat-surface geometry. Because the commercial EMAT has minimal contact surface area with the pipe, excitation of shear waves in non-ferromagnetic stainless steel is not efficient. Figure 23 shows custom-made EMAT,

in which the same array of magnets is arraigned such that the surface is contoured to match the pipe curvature. A flexible wire-coil can be placed on top of the custom array of magnets to generate shear waves in the same way as that in the commercial EMAT. The custom EMAT is expected to generate stronger signal in the pipe compared to the flat-surface commercial EMAT.

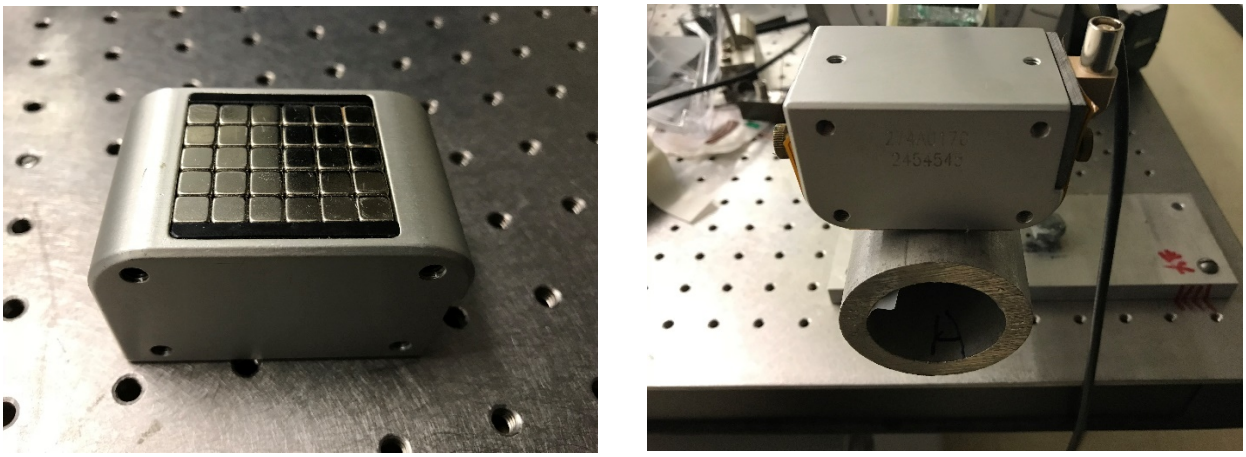

Figure 22 – Commercial EMAT with coil removed showing an array of magnets. Flat surface of EMAT has minimal contact with the pipe.

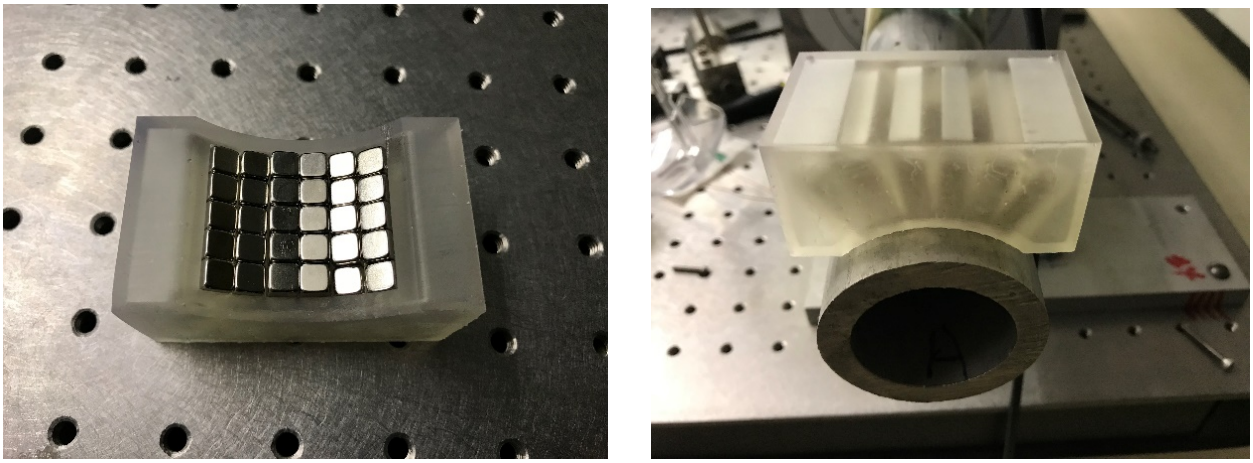

Figure 23 – Custom-made EMAT with contoured surface to match pipe curvature.

4. Description of Software Defined Radio Protocol for Acoustic Communication on Pipes

4.1. Introduction

Data of interest for transmission on nuclear reactor pipes includes sensor readings, voice, and images. Transmission of images is most challenging because corruption of the header string might render the reconstructed image unreadable. We used the Software Defined Radio (SDR) tool GNURadio, which allowed us to build a communication protocol to transmit data effectively. We created a Python tool to compare different modulation and front error correction techniques used to transferring header files. The goal of this task was to successfully transmit the header file of a .ppm (Portable Pixel Map) image because any corruption in this data renders the image useless.

For the physical transmission, we employed two ultrasonic PZT's on a six foot-long stainless steel pipe spaced at about five feet apart. The transducers were originally designed for nondestructive testing. A digital wave is generated by the GNURadio program, which is next converted into an analog wave by Red Pitaya electronic boards. This analog wave is sent to the PZT through an amplifier, which converts the electronic wave into an acoustic wave by vibrating PZT crystal at a certain frequency. This vibration passes through the pipe in the form of a shear mechanical wave and vibrates the transducer on the other end of the pipe, generating an electrical wave, which is converted back into a digital wave by Red Pitaya.

4.2 Modulation Techniques

Digital modulation is the process sending a binary signal inside of a different signal that can be easily transmitted over a physical channel. In our case, we chose to employ binary Amplitude Shift Keying (ASK) and binary Phase Shift Keying (PSK). Schematics of shift keying modulation techniques are displayed in Figure 24.

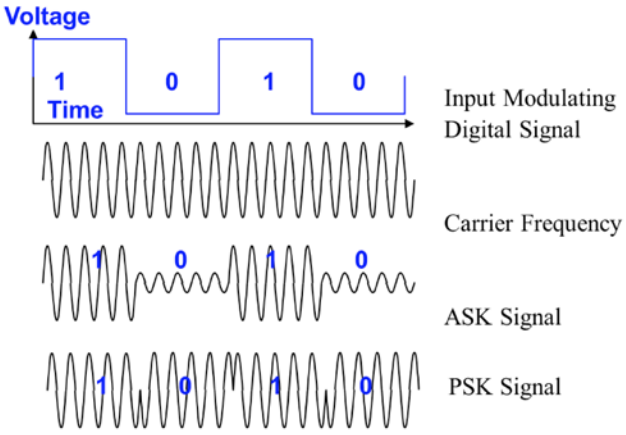

Figure 24 – Schematics of shift keying modulation techniques

In ASK, a 1 is represented as a high amplitude, and a 0 is represented by a low amplitude. In PSK, a 1 is represented by a 180 degree phase shift on the carrier frequency, and a 0 is represented by a 0 degree phase shift on the carrier frequency. The binary waveform is multiplied onto a carrier frequency, produced by the Red Pitaya, and transmitted through the pipe. On the receiving end, the signal is demodulated by multiplying again by the carrier frequency and passing the information through a low pass filter to recover the original signal. These are the most simple forms of modulation available, and while more elaborate forms of Shift Keying exist that allow for more information to be encoded per key, we chose this technique due to the fact that the constellation symbols are maximally spread out, reducing the impact of noise on the channel compared to a setup that encodes more than one bit per symbol.

4.3 GNURadio Communication Protocol Implementation

In communication protocol implemented in SDR, image data has to be processed in order to be successfully transmitted and recovered. As noted above, only a binary stream of information can be sent through the pipe. However, image data has a non-binary data structure and for that we have chosen to use a Portable Pixel Map (PPM) file as our primary image data structure for transmission. Table 3 lists an examples of a header file.

Table 3 – Example of header file

P3	<- file type
4 4	<- dimensions in pixels
255	<- maximum pixel value (rgb is 0 to 255)
1 1 0	
4 1 2	
5 3 4	

The PPM file type stores the image dimensions in the first three lines and the rest is the image itself as a matrix after that in the form of ASCII character. We will refer to these three lines as the “image header” and the rest as the “image payload”. The image header is critical to successful recovery of the image, as if there are any errors within the file, the computer will not be able to read the data effectively. The image payload, on the other hand, can contain more errors as a single error is less likely to make the file unreadable.

To transmit this information, data structure has to be converted into binary, sent, and reassembled back into its original form. To accomplish this task, we first disassemble the file into a stream of ASCII characters, in the form of bytes (1 byte = 8 bits). Table 4 below shows ASCII values of select characters.

Table 4 – ASCII to number conversion table

ASCII value	Character	ASCII value	Character	ASCII value	Character
000	^@	043	+	086	V
001	^A	044	,	087	W
002	^B	045	-	088	X
003	^C	046	.	089	Y
004	^D	047	/	090	Z
005	^E	048	0	091	[
006	^F	049	1	092	\
007	^G	050	2	093	]
008	^H	051	3	094	^
009	^I	052	4	095	_
010	^J	053	5	096	`
011	^K	054	6	097	a
012	^L	055	7	098	b
013	^M	056	8	099	c
014	^N	057	9	100	d
015	^O	158	:	101	e
016	^P	059	;	102	f
017	^Q	060	<	103	g
018	^R	061	=	104	h
019	^S	062	>	105	i
020	^T	063	?	106	j
021	^U	064	@	107	k
022	^V	065	A	108	l
023	^W	066	B	109	m
024	^X	067	C	110	n
025	^Y	068	D	111	o
026	^Z	069	E	112	p
027	^[	070	F	113	q
028	^\	071	G	114	r
029	^]	072	H	115	s
030	^^	073	I	116	t
031	^-	074	J	117	u
032	[space]	075	K	118	v
033	!	076	L	119	w
034	"	077	M	120	x
035	#	078	N	121	y
036	$	079	O	122	z
037	%	080	P	123	{
038	&	081	Q	124	|
039	'	082	R	125	}
040	(	083	S	126	~
041	)	084	T	127	DEL
042	*	085	U		

These characters are then converted into a bit stream, a packet header is attached and is passed through the modulation methods mentioned earlier. After being demodulated, the bit stream is parse to remove the packet header, the bits are converted into their original bytes, and the file is reassembled. When error correction is added, after the bytes are converted into bits they are multiplied by a convolution matrix, and once received, the bits are deconvoluted by an inverse matrix. Overall, the protocol of the communication system was the primary focus of this project as reducing the number of errors in transmitting ensures that the communication system is reliable.

GNURadio environment was used to develop and implement the communication protocol. Figure 25 below displays a flowgraph generated by GNURadio for ASK modulation with no convolutional code. Descriptions of various blocks functionalities are provided in tables below.

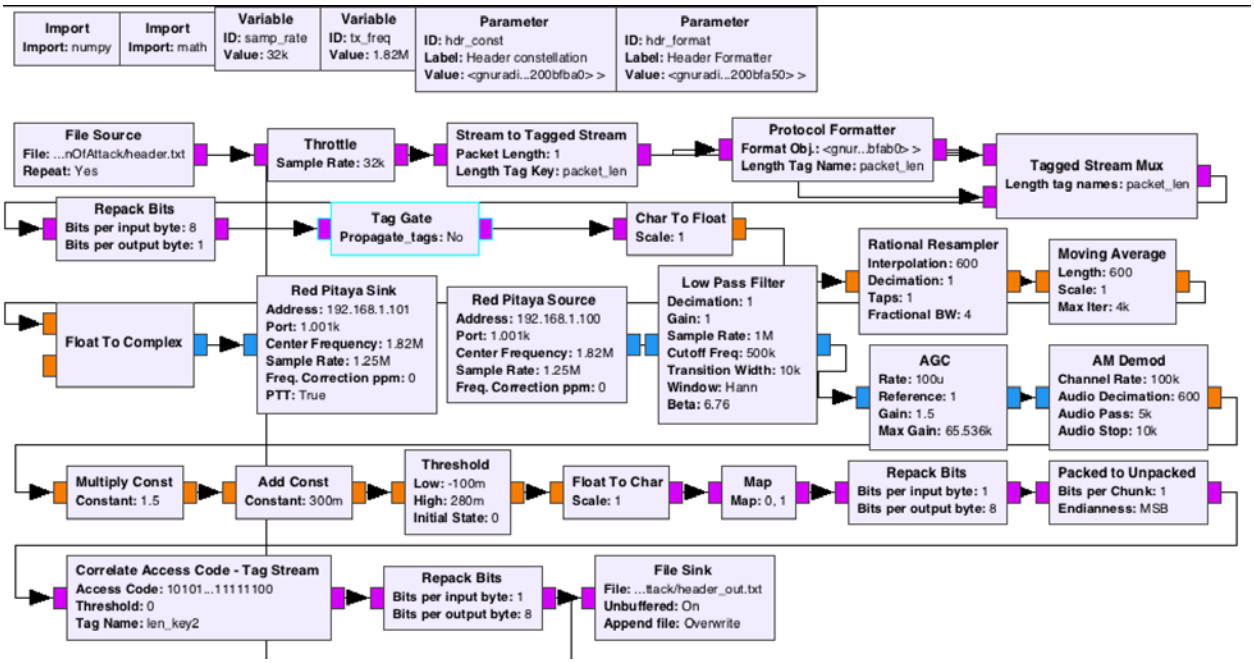

Figure 25 – ASK acoustic communication protocol flow chart created by GNURadio

Explanations of blocks functionalities before modulation, during modulation, and after modulation steps are provided in Tables 5, 6 and 7, respectively.

Table 5 – Functionalities of blocks before signal modulation steps

Block	Input	Output	Parameters	Actions	Purpose
File Source	Text file containing information to be sent	Characters in the file in form of continuous stream of bytes	Output type: Whether the file is a stream of bytes, floats, ints, etc; Repeat: Whether the file will be infinitely repeated;		Opens the needed data file
Throttle	-	-	Sample Rate: Number of samples per second	Limits the flow of information to 32k samples/sec	Makes sure computer doesn't overheat
Stream to tagged stream	Continuous stream of characters	Continuous stream of characters with tagged	Packet Length: Controls how much data stored is per packet		Puts a marker on the start of a packet for the header generator to attach to
Protocol Formatter	Continuous tagged stream of characters	String of header characters	Formater Obj: Sets the protocol formatter's key parameters: Preamble and Access Code, which are basically what the correlate access code will look for when assessing what is a packet	Creates a header for the packet	
Tagged Stream Mux	Two tagged streams	One tagged stream	Length tag names: Input the length of the data stream to which to attach the header	Combines the two data streams by putting input 1 in front of input 2	
Repack Bits	1 byte	8 bytes	Length tag name: Input the length of the data stream, Packet Alignment: How packets are aligned, Endianness MSB or LSB (which one comes first in stream)	Converts the stream of bytes into a stream of bits	Modulation techniques deal with bits and not bytes

Table 6 – Functionalities of blocks during signal modulation steps

Block	Input	Output	Parameters	Actions	Purpose
Char to float	Character	Float	Scale: Ratio of Char value to Float value	Converts a character value of -128 to 127 (0 and 1 in this case as we are in BITS) to its numeric value	Numbers are sent through the channel, not characters
Rational Resampler	1 float	600 floats	Interpolation: How many samples to add to the stream	Creates a digital square wave out of single points	We use a square wave to transmit data
Moving Average	Input is a stream of floats	Output is the moving sum of the last N samples, scaled by the scale factor	Length of averaging window, number to divide by, max number of iterations in averaging	Sums the last N points, to be divided by the scaling factor. This is	
Float to Complex	Float	Complex	Scale factor	Converts float to complex number (magnitude)	Succeeding blocks use complex numbers
Red Pitaya Sink	Complex	None	Address: IP address of red pitaya to connect to; Port: Connection port; Center frequency: Frequency by which the red pitaya multiplies the square wave by (important as this is the frequency at which the transducer oscillates); Sampling rate: Sampling rate of the red pitaya (basically we want this as high as possible to give the most accurate waveform)	Transmits the data to the transducer	Acts as a digital (discrete) to analog (continuous) converter and a fir filter
Red Pitaya Source	None	Complex	Address: IP address of red pitaya to connect to; Port: Connection port; Center frequency: Frequency by which the red pitaya multiplies the square wave by (important as	Receives the data from the transducer	Acts as an analog (continuous) to digital (discrete) converter and

			this is the frequency at which the pzt oscillates); Sampling rate: Sampling rate of the red pitaya (basically we want this as high as possible to give the most accurate waveform)		a fir filter
Low Pass Filter	Complex	Complex	Cutoff frequency: Frequency to attenuate	Attenuates above a threshold frequency	Removes high frequency noise as well as any carrier frequency to leave square wave
Active Gain Control (AGC)	Complex	Complex	The gain is updated by the equation: Gain = Gain + Rate * (Reference - abs(Input)); Max Gain: the automatic gain will not exceed this value. If set to 0 there is no max	Applies gain loop onto signal	Stabilizes the signal for demodulation
AM Demod	Complex	Float	Channel_rate – incoming sample rate of the AM baseband; audio_decim – input to output decimation rate (integer); audio_pass – audio low pass filter passband frequency (float); audio_stop – audio low pass filter stop frequency (float)	Demodulates the signal	Decimates the square wave
Multiply Const	Float	Float	Number to multiply by	Multiplies by a constant	Fine tuning
Add Const	Float	Float	Number to add	Adds a number	Fine tuning
Threshold	Float (range of values)	Float (1 or 0)	Upper threshold, lower threshold	The output transitions from 0.0 to 1.0 when the input signal transitions from below to above the High level. The output transitions from 1.0 to 0.0 when the input signal transitions from above to below the Low level.	The thereshold converts the stream of floats into binary (bits)

Table 7 – Functionalities of blocks after signal modulation steps

Block	Input	Output	Parameters	Actions	Purpose
Map	Float	Float	Map of values to send to	Maps incoming data to 0 or 1	Makes sure that data is mapped to bits
Repack Bits	8 bytes	1 byte	Length tag name: Input the length of the data stream, Packet Alignment: How packets are aligned, Endianness MSB or LSB (which one comes first in stream)	Converts the information from bits into bytes	Byte manipulation technique
Packed to Unpacked	1 byte	8 bytes	Endianness MSB or LSB (which one comes first in stream)	Converts the bytes into bits	The correlate access code deals with bits, not bytes
Correlate Access Code	Continuous stream of bits	Continuous stream of bits without header bits	Preamble and Access Code: What the correlate access code will look for when assessing what is a packet	Removes the header bits from the bit stream	The original data has no header bits, so we want to remove them
Repack Bits	8 bytes	1 byte	Length tag name: Input the length of the data stream, Packet Alignment: How packets are aligned, Endianness MSB or LSB (which one comes first in stream)	Converts the bits into bytes	Original data was stored as characters, not bits
File Sink	Continuous stream of characters	None	Input type: What kind of information is being written to file; Unbuffered: Whether or not the file is being buffered; Append file: Whether the incoming data overwrites the old file or append it.		Saves the incoming file

4.4 Communication Protocol Testing and Analysis

To compare different data transmission techniques, a simple message was passed through the system and monitored in each GNURadio flowchart block. In this example, we send a file with characters “!s!” for demonstration purposes. We will follow the journey of a packet as it is transmitted through the system. Below is a representation of what occurs at each step in the process.

In the file source block, we see how file is being disassembled into three values: 33, 115, 33. The value of 33 corresponds to “!” and the value of 115 corresponds to “s”. Figure 26 below displays the raw data and each character labeled as a separate color.

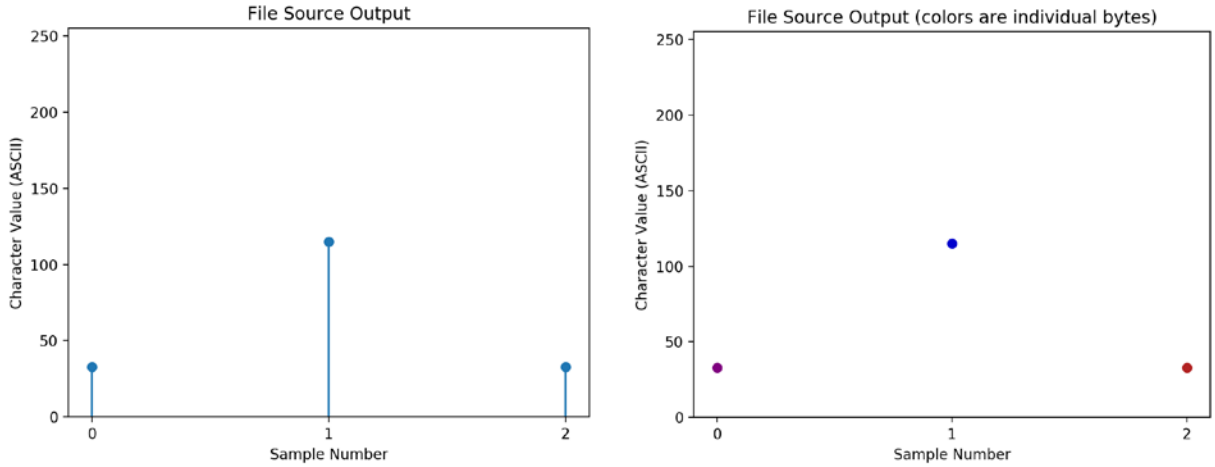

Figure 26 – File source output (left) raw data, (right) data colored as individual bytes

The protocol formatter block creates a tagged stream of 1’s and 0’s that will be attached to the payload. In our case, we use the default preamble of '1010010011110010' and access code of '10101100110111011010010011100010111100101000110000100000111111100', which is displayed above as bytes in Figure 27 (raw data and data colored as bytes)

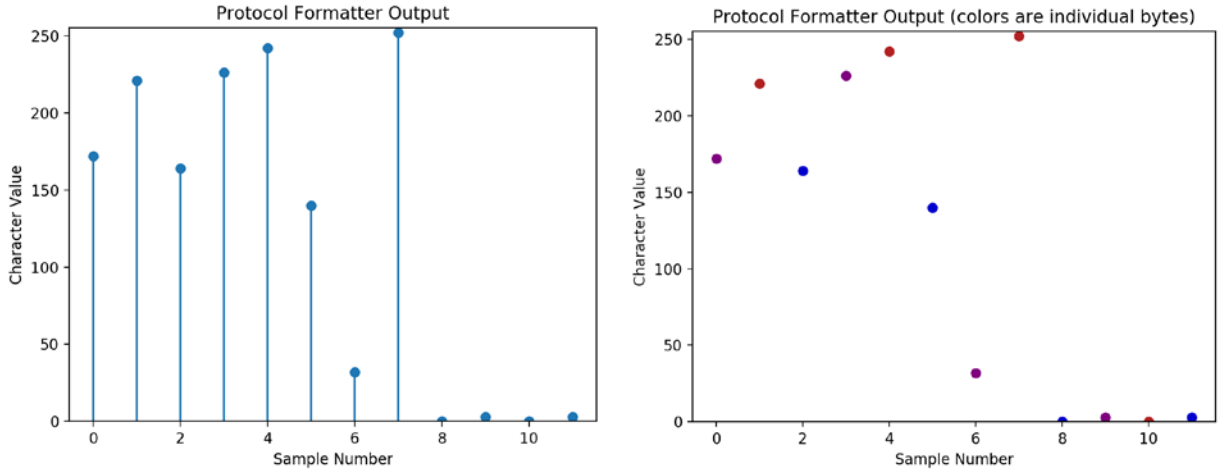

Figure 27 – Protocol formatter output (left) raw data, (right) data colored as individual bytes

Figure 28 below visualizes how the header file is combined with the payload. We first see the attached preamble in the form of bytes. The first 12 bytes are from the protocol formatter while the last 3 are from the file source. Specifically, we can see that bytes 12, 13, 14 match the file source.

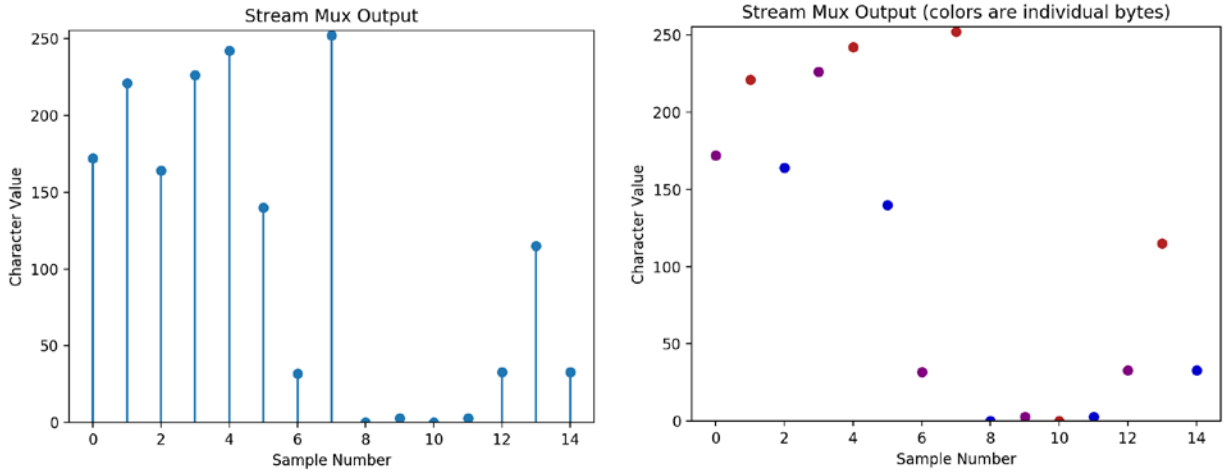

Figure 28 – Stream mux output (left) raw data, (right) data colored as individual bytes

We can now see how after the stream mux, we unpack the individual bytes into 8 bits each. The individual bytes are displayed above with colors corresponding to each byte in Figure 29. There are 15 bytes in total for the packet, meaning that we are now sending 120 samples through the system (15*8=120)

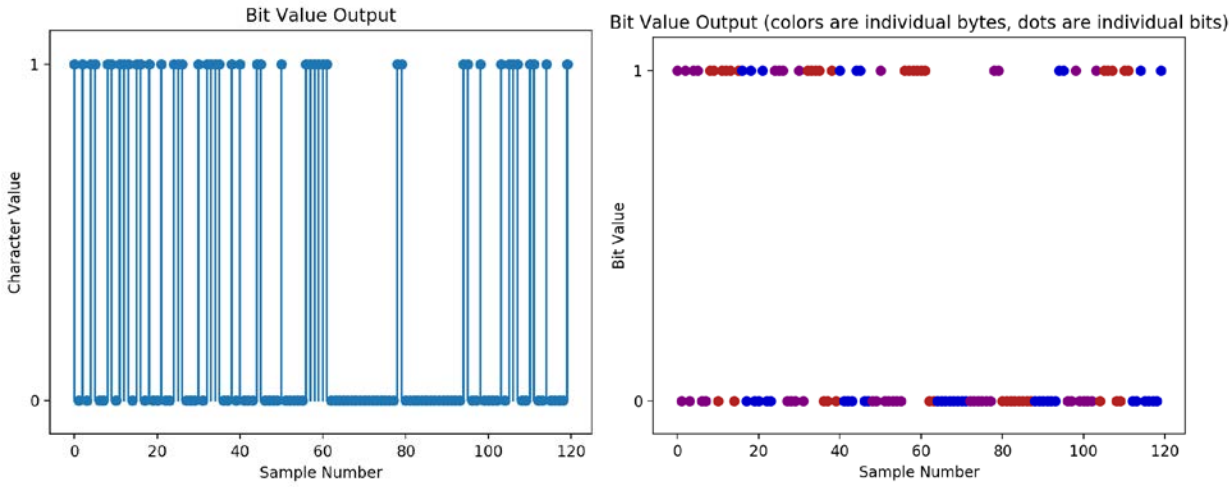

Figure 29 – Bit value output (left) raw data, (right) data colored as individual bytes

Figure 30 below shows a zoomed-in view of the first byte in the stream. We can see that it does in fact correspond to the character value of 172, since $10101100 = (1 \times 2^7) + (0 \times 2^6) + (1 \times 2^5) + (0 \times 2^4) + (1 \times 2^3) + (1 \times 2^2) + (0 \times 2^1) + (0 \times 2^0) = 172$.

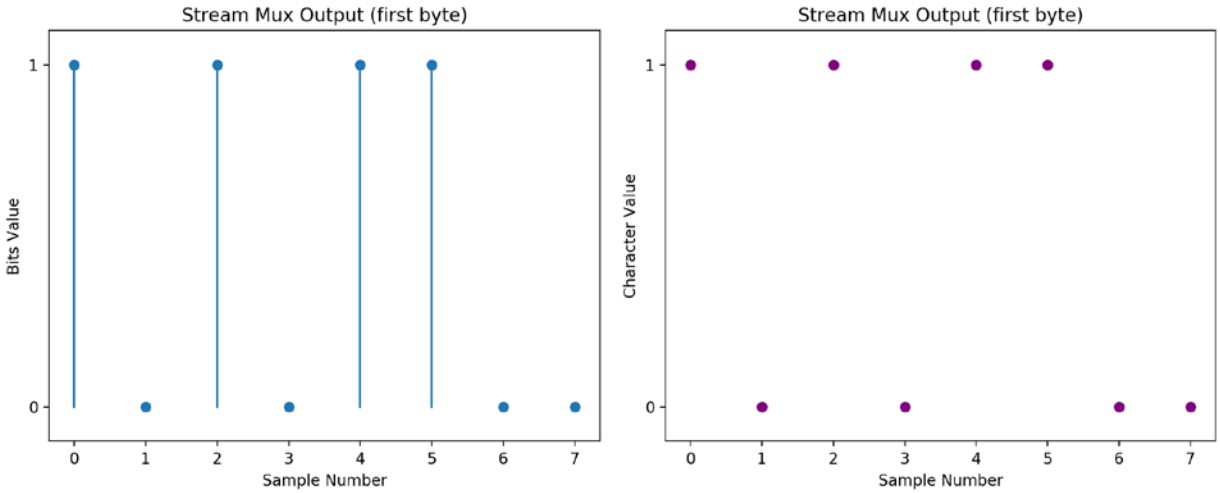

Figure 30 – First byte stream mux output (left) raw data, (right) data colored as individual bytes

Figure 31 below shows what happens to the information after the rational resampler and moving average block. Each bit is interpolated to create 600 bits after it, which is why the total number of samples goes from 120 in the figure with the data displayed as bits, to 72000 in the above figures (120*600=72000). In both graphs, we can see how the signal is converted from digital to analog, transforming the latter into a square wave.

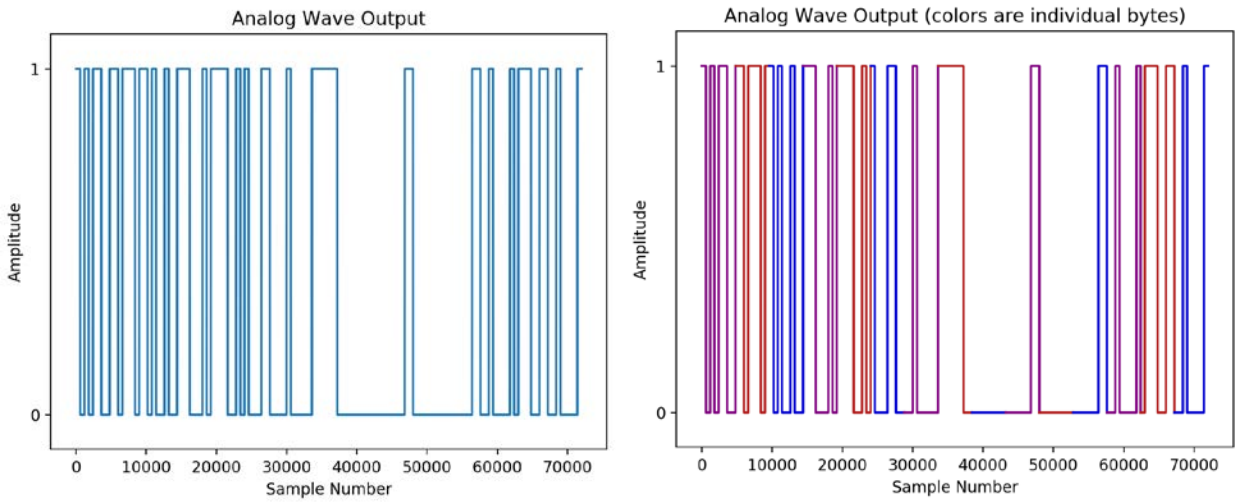

Figure 31 – Analog wave output (left) raw data, (right) data colored as individual bytes

Figure 32 below displays Fast Fourier Transform (FFT) digital calculation of the analog wave output spectrum. The bandwidth of the signal is less than 50KHz.

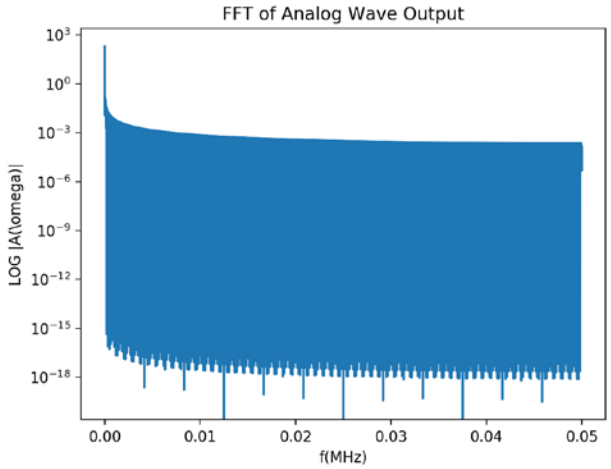

Figure 32 – FFT spectrum of analog wave output

Figure 33 below displays the data taken from the oscilloscope at a sampling rate of 25 Ms/s, which is much higher than GNURadio's rate of 100 ks/s, which is why the number of samples for the same signals is 250 times higher than in GNURadio (250*100,000=25,000,000). The individual bytes from the square wave are all translated into a signal with amplitude ranging from -0.3 to 0.3 volts. Note that in our setup we pass this signal into a 50 dB amplifier, the transducer actually feels a voltage of about 95 volts. We can see that Red Pitaya introduces ringing into the system on every on/off voltage high/low. This kind of behavior is why we chose to use binary ASK over quad ASK, since this kind of instability only lends itself to on or off keying.

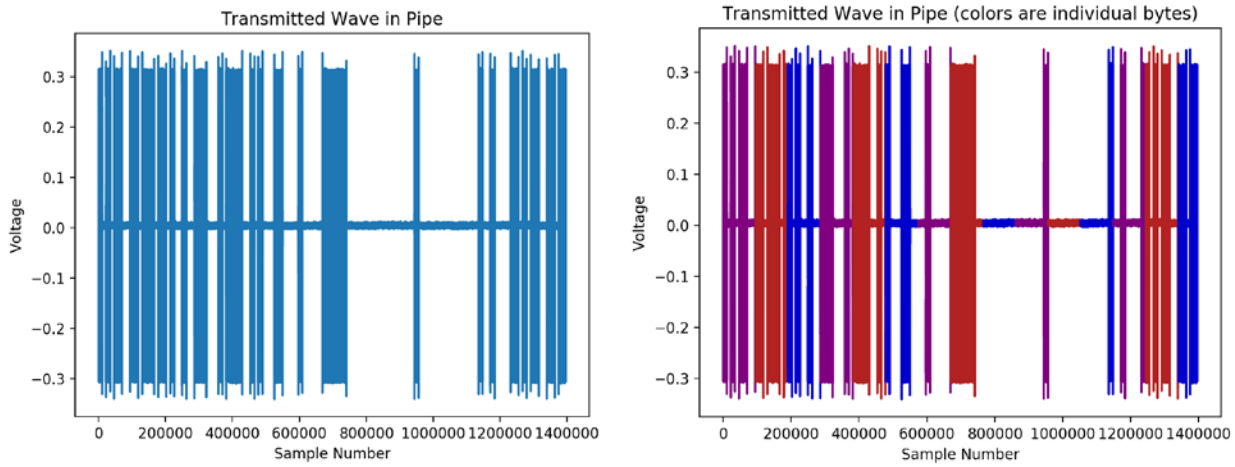

Figure 33 – Transmitted wave on pipe (left) raw data, (right) data colored as individual bytes

Figure 34 below displays FFT spectrum of the transmitted signal on pipe. Compared to the spectrum of the analog output signal in Figure 10, we see that the frequency response of the square wave is still seen on the lower end of the spectrum, and we can also clearly see the carrier frequency centered at 1.8 MHz. We can see that the frequency response of the carrier frequency is stronger than the frequency response of the base band.

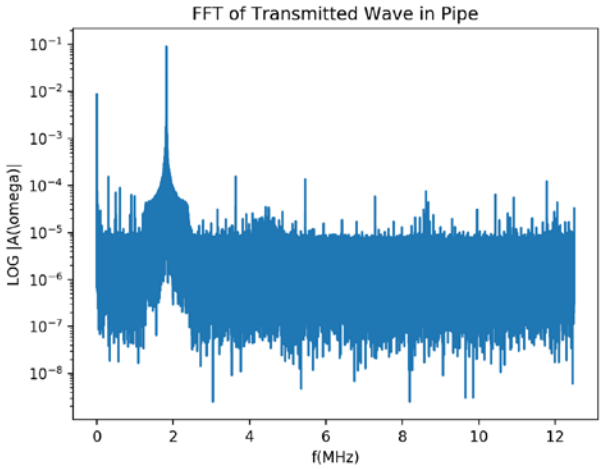

Figure 34 – FFT spectrum of transmitted wave of pipe

Figure 35 displays the received signal waveform before demodulation. The data is obtained from the oscilloscope, which is now connected to the output of the low noise amplifier placed after the receiving transducer. We can see that the signal, even with the use of two amplifiers, is attenuated by 10 and in addition, a DC offset of -0.075 volts is added to the signal. Compared to the

transmitted signal, we can see more distortion along the peaks of the signal, as well as a much larger amount of noise around the DC offset.

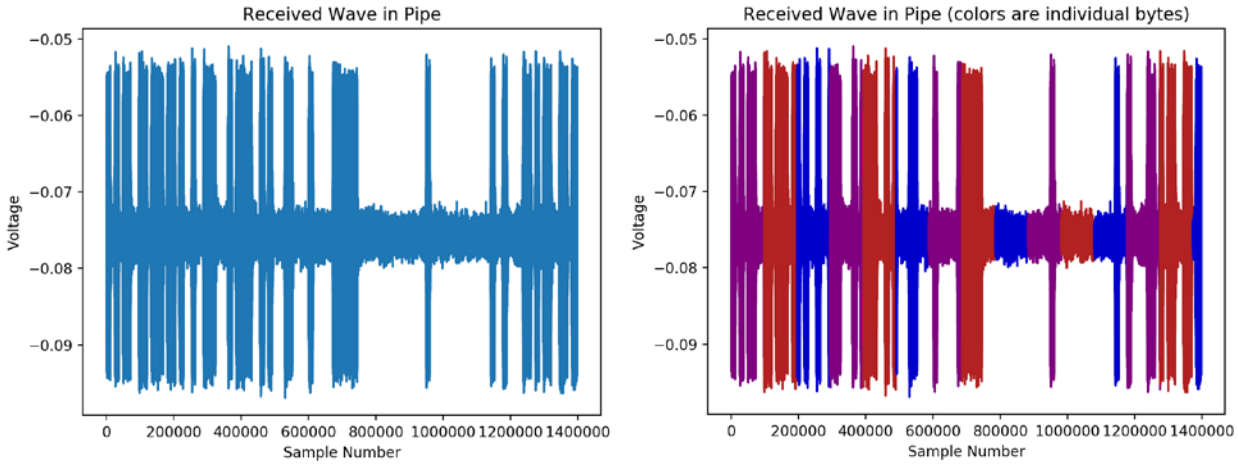

Figure 35 – Received wave on pipe before demodulation (left) raw data, (right) data colored as individual bytes

Figure 36 displays the frequency spectrum of the received waveform before demodulation. Compared to the transmitted signal spectrum shown in Figure 34, we can see that the frequency response of the baseband is higher than the frequency response of the carrier frequency.

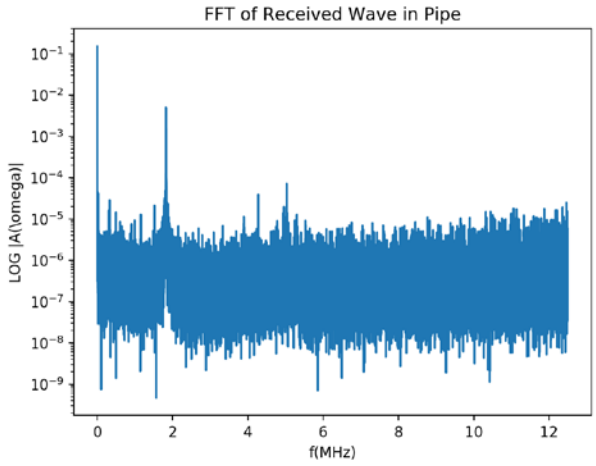

Figure 36 – FFT spectrum of received wave on pipe before demodulation

Figure 37 below displays of the first byte in the string of characters in the received signal in Figure 35. We see that after the shift keying has been switched to the off position, we still see some ringing from the waveform.

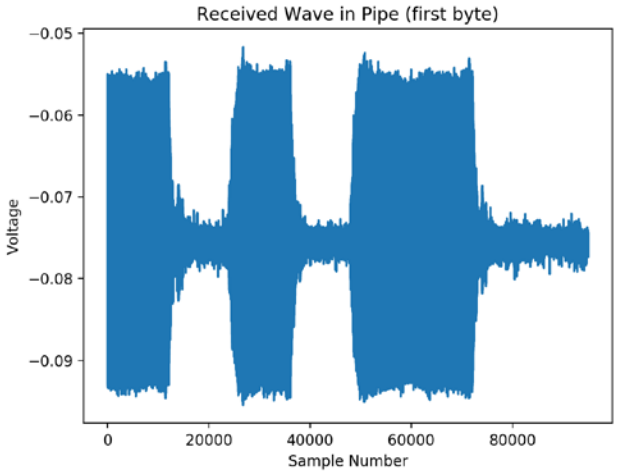

Figure 37 – First byte in received signal before demodulation

Figure 38 below is the received demodulated signal with Red Pitaya board, displaying the repeated string of characters. We see that at first the system produces information that cannot be decoded (Sample number <500000), but then proceeds to produce a waveform that is more stable. Since our sample rate is 100000 S/s, we can therefore conclude that the system has to transmit for 5 seconds before the information can be processed successfully. The overall shape of the incoming signal envelope has a sinusoidal shape, suggesting that there is a phase mismatch between the transmitting Red Pitaya and the receiving Red Pitaya boards.

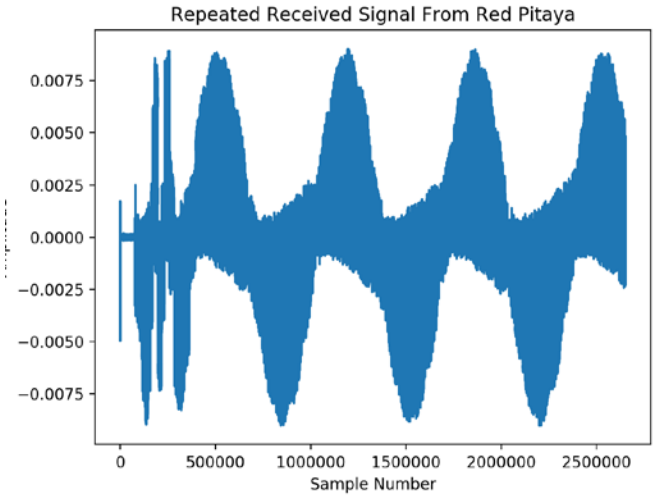

Figure 38 – Received demodulated signal with Red Pitaya board

Figure 39 below displays FFT spectrum of the demodulated received signal, which should be matching that of the transmitted analog square wave in Figure 32. We can see that the frequency

roll off is similar to that of the transmitted information, however the frequency response is not as smooth as in the transmitted signal.

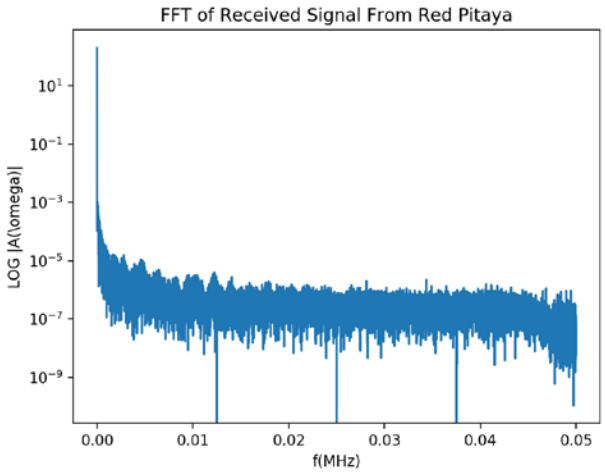

Figure 39 – FFT spectrum of demodulated signal received with Red Pitaya board

Figure 40 below provides a zoomed in version of the character transmission of the received signal from Red Pitaya board. If we compare this plot to the transmitted waveform in Figure 33, we can see that there is much more ringing in the received signal compared to the transmitted one. This result matches that of the frequency response, as we can see that the imbalanced frequency response makes the square waves less defined.

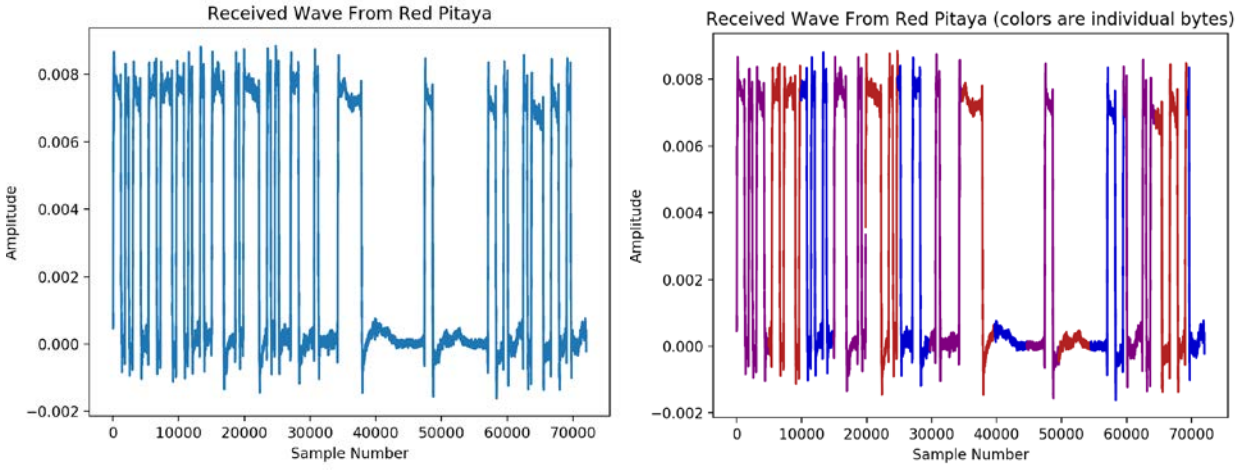

Figure 40 – Zoomed-in received signal from Red Pitaya board (left) raw data, (right) data colored as individual bytes

Figure 41 below displays a plot of the signal as it passes through the automatic gain control (AGC). We can see that this signal has the same shape as that of the signal that exits Red Pitaya, however

the amplitude is increased. This is done to prepare the signal for the threshold section, which needs a greater difference in amplitude between on and off states representing digital “0” and “1”

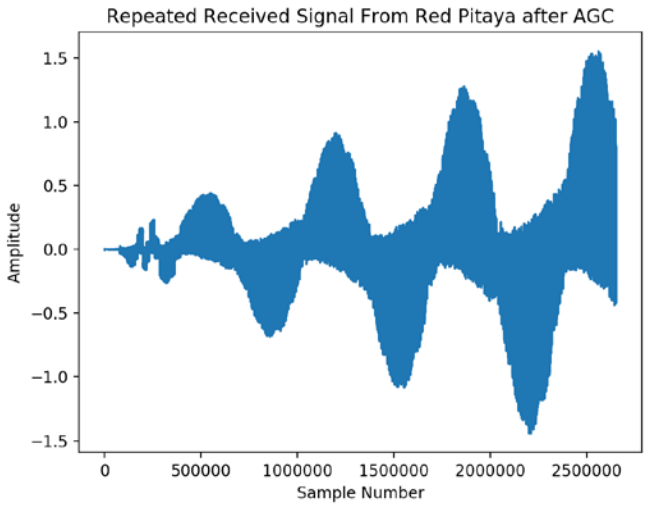

Figure 41 – Signal amplification with automatic gain control (AGC)

AGC is needed to compensation of demodulated signal amplitude reduction due to random phase difference in the received and reference waveforms. The average or peak output signal level is used to dynamically adjust the gain of the amplifiers, enabling the circuit to work satisfactorily with a greater range of input signal levels, so that we can set a proper up threshold for ‘1’ and down threshold for ‘0’. the AGC effectively reduces the amplitude if the signal is strong and raises it when it is weaker. Implements an automatic gain control with a single rate parameter for both attack and decay. The gain is updated by the equation

$$Gain = Gain + Rate * (Reference - abs(Input)) \quad (12)$$

The equation is for each sample.

- Attack rate – how fast the AGC decreases the gain when a loud signal appears
- Decay rate – how fast the AGC increases the gain when the loud signal is gone
- Reference – This is the level the AGC will try to maintain

Figure 42 below displays the data of threshold block after demodulation. We can see that the system can only begin to recognize the bits after a certain number of samples have passed, showing that the active gain control needs time to grow before being demodulated.

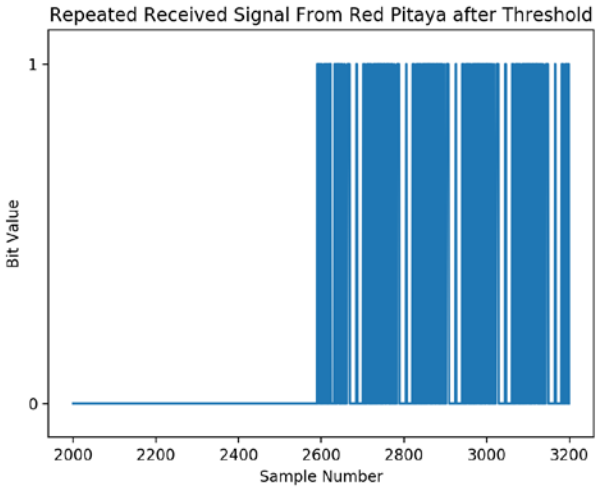

Figure 42 – Data of threshold block after demodulation

Figure 43 below displays information recovered from the threshold block after decimation. We see that the recovered information follows the same pattern as the transmitted bits.

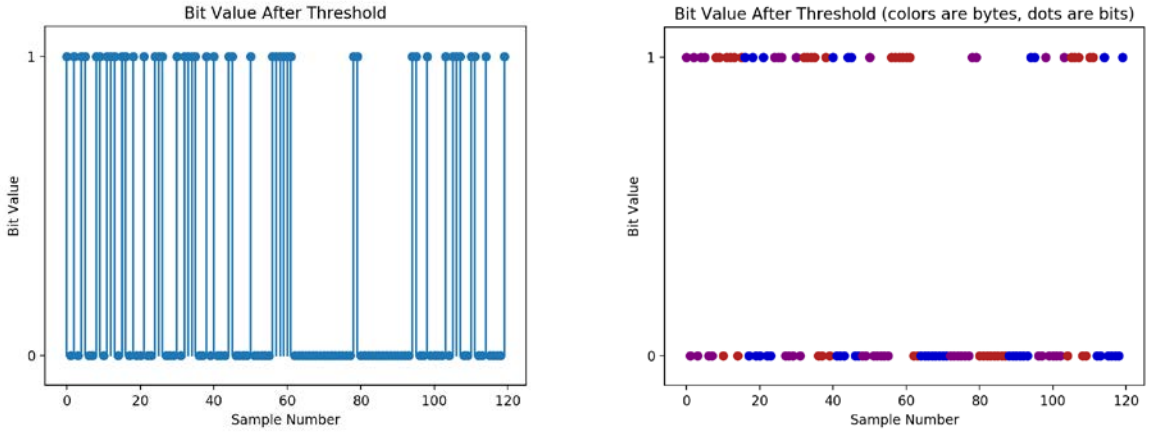

Figure 43 – Data recovered after decimation (left) raw data, (right) data colored as individual bytes

The correlate access code removes the bits from the stream that follow originate from the protocol formatter, leaving the original information. Figure 44 below displays the resulting data bits

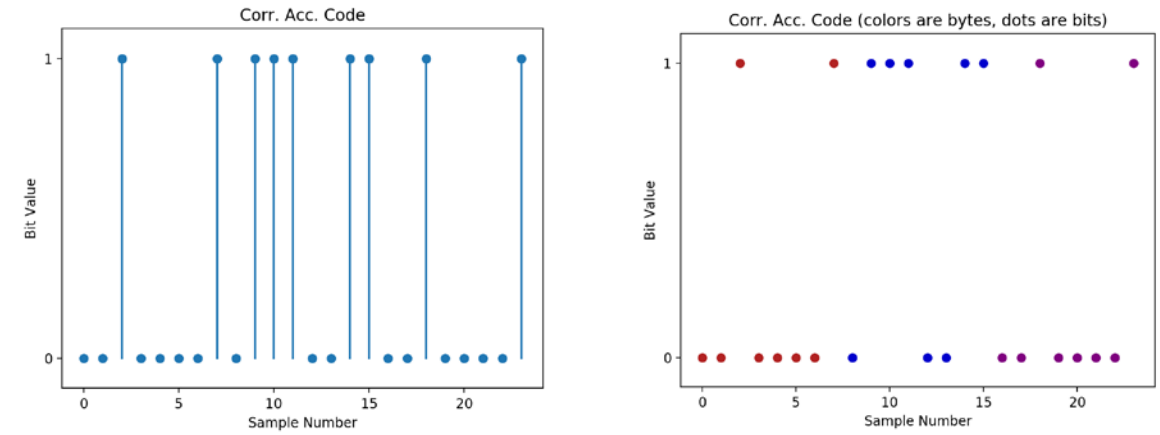

Figure 44 – Data recovered with correlated access code (left) raw data, (right) data colored as individual bytes

The repack bits block repacks the bits into bytes and stores the information into the file sink, successfully recovering the transmitted file. The data is displayed in Figure 45 below.

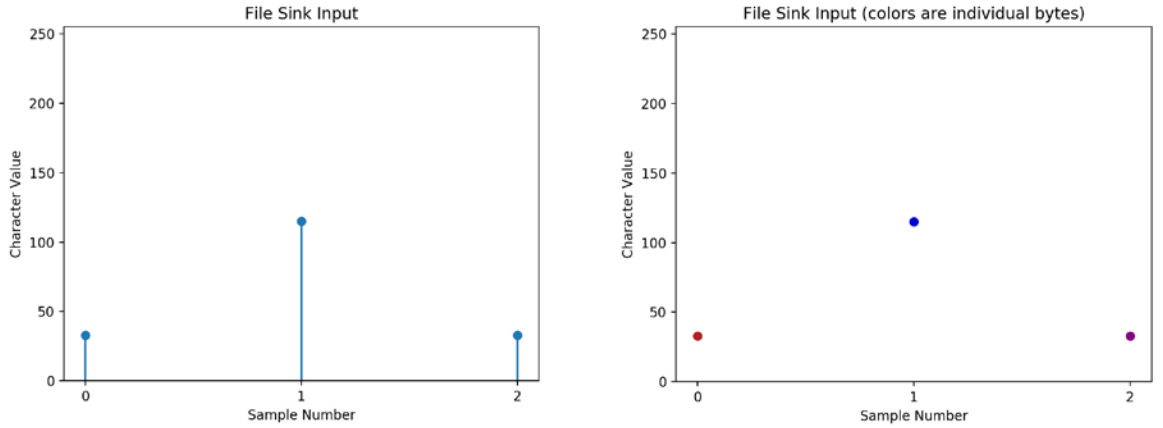

Figure 45 – Data from file sink input (left) raw data, (right) data colored as individual bytes

4.5 Comparison of Communication Protocols Performance

To quantify differences in performance of ASK and PSK communication protocols, we developed a Python script that transmitted a string of characters, similar to that of an image header file. Data was transmitted with different combinations of modulation and error correction. We then compared the number output by the file source against the input of the file sink to see how effectively the data was transmitted.

The Python code considers 4 combinations of communication channels: ASK (Amplitude Shift Keying), ASK with CC (with Convolutional front error Correction), PSK (Phase Shift Keying), PSK with CC. We ran a simulation channel that modified the SNR (Signal to Noise Ratio) by adding various voltages of AWGN (Additive White Gaussian Noise). Figure 46 displays bit error rate (BER) in header file transmission vs. signal to noise ratio (SNR) in units of dB.

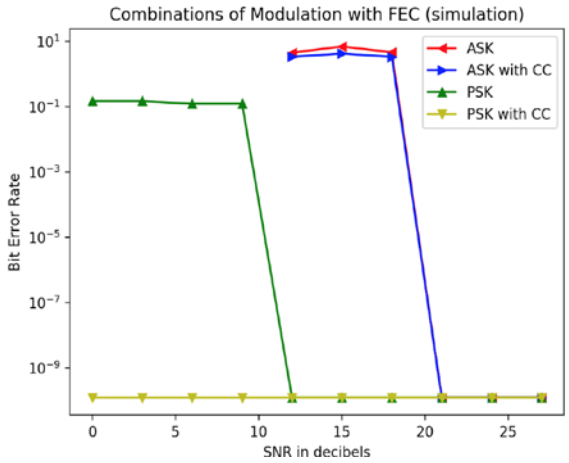

Figure 46 – BER vs. SNR for ASK, ASK with CC, PSK, and PSK with CC schemes

Overall, we see that the most effective method of communication in simulation is PSK with CC, which was successful at transmitting at all SNR levels. PSK was also effective, with the bit error rate dropping sharply after 10 decibels. The CC technique appears to slightly increase the performance of ASK modulation.

However, due to experimental limitations, the analog to digital converter was not capable of effectively demodulating the signal transmitted through the pipe. Therefore, instead ASK and ASK with CC were tested. The results are plotted in Figure 47 as BER vs carrier frequency. Interestingly, ASK either transmits perfectly or not at all at different frequencies while ASK with CC transmits at all frequencies, abet with a high error rate. Both techniques work at 2 MHz, which suggests that the communication system prefers higher frequencies.

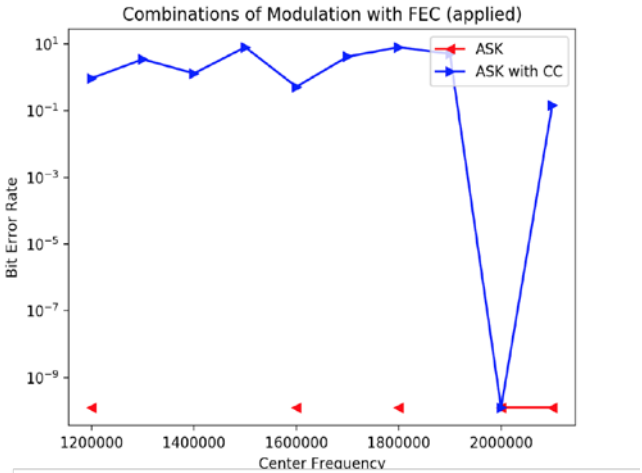

Figure 47 – BER vs. carrier frequency for different ASK and ASK with CC schemes

4.6. Demonstration Data Transmission with PZT-based Channel

Demonstration image, text and sound transmission on a CVCS-type pipe with baffle plates using Red Pitaya boards and GNURadio software was performed during the Digital Environment for Advanced Reactors Workshop at ANL (Heifetz 2018). In the final demonstration, information transmission with 1.8MHz frequency shear wave at 2KB/s data rate across 5 feet distance on stainless steel pipe. Figure xx show schematic of data transmission architecture and the laboratory photograph. Demonstration included transmission of an image with ANL logo (32KB of memory of computer hard drive) at 2KB/s data rate. Schematics of the communication system setup for transmission of images and laboratory photograph of the setup are shown in Figure 48

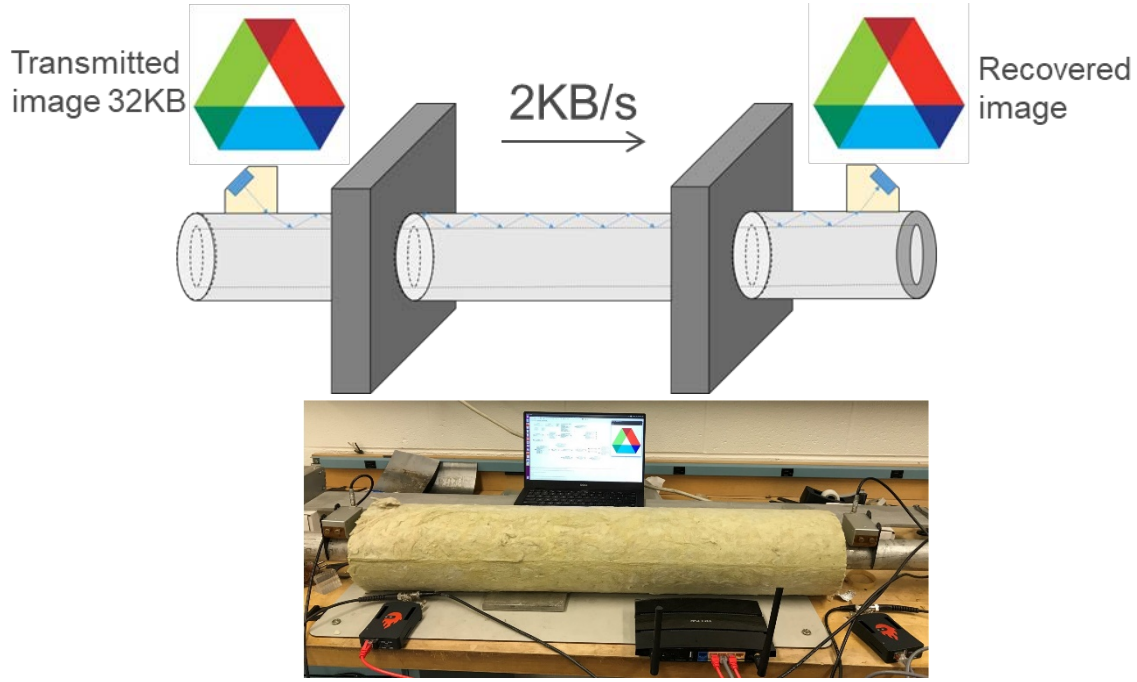

Figure 48 – Schematics of communication system setup for image transmission on a pipe (top) and laboratory photograph of the setup (bottom)

An example of text file transmitted using the same communication setup is shown in Figure 49. The left panel displays the contents of transmitted file containing the string “Hello world!” The string is continuously transmitted. The right panel of the same figure contains multiple instances of the received string. Note that no errors can be observed in repeated transmission trials.

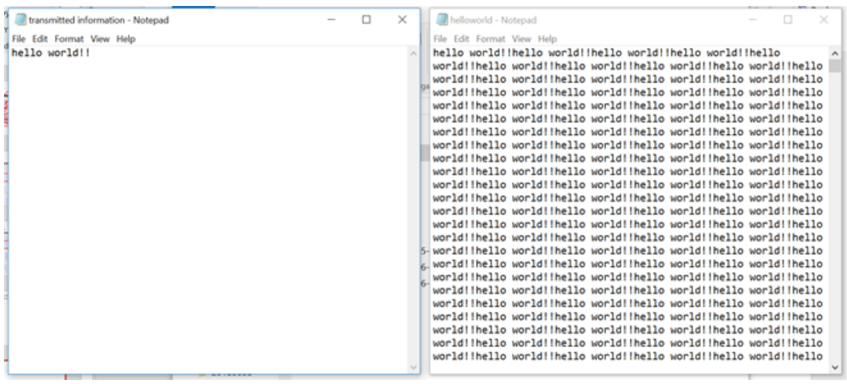

Figure 49 – Transmission of text (left) transmitted file, (b) received file

5. Conclusions

The objective of this project is to develop and demonstrate methods for transmission of information in nuclear facilities across physical barriers as acoustic/elastic guided waves along existing in-place metal piping infrastructure. In this report, we discuss acoustic communication system design considerations, including data transmission requirements for a nuclear facility and transducer operating conditions. A viable candidate for acoustic communication channel is a chemical volume control system (CVCS) stainless steel pipe, which penetrates through the containment building wall. A laboratory bench-scale system consisting of a nuclear grade CVCS-like pipe and ultrasonic transducers was assembled for a preliminary communication system analysis.

Because of limited bandwidth of ultrasonic transducers, on-off-keying OOK digital communication protocol was chosen for information transmission over an acoustic channel. Design considerations of the OOK communication protocol are intimately connected to physical characteristics of the communication channel. This report addresses acoustic channel characterization through computer modelling of elastic wave coupling and propagation in the transducer/piping structure using COMSOL^{TM} software package. Computer simulations were performed to provide theoretical support to results obtained in laboratory experiments on signal transmission with elastic shear waves on a pipe. In particular, computer models provide qualitative analysis of coupling losses and communication signal noise due to multiple scattering at the wedge/pipe interface. Also, 3-D simulations indicate that refracted shear wave a pipe generated with an angled wedge are torsional waves, In addition, proof-of-principle experimental studies were conducted to investigate performance of communication link under the conditions closely resembling a representative scenario. Anchoring baffle plates were added to the basic setup, and low frequency process noise was simulated by mechanically shaking the pipe. Acoustic communication system was shown to be resilient against such interferences. . In case of hardware resource improvements, the tradeoff between transducer frequency and attenuation losses will be further investigated. In principle, losses in the channel can be compensated with low noise amplifier, so this additional constraint will be factored into design consideration. Also, attenuation in the channel could be potentially used to the benefit of communication system by suppressing echoes. Finally, custom geometry EMAT is under development to improve the efficiency of signal coupling into the pipe.

Communication protocol was developed in GNURadio software defined radio (SDR) environment, with interface to Red Pitaya electronic boards. Transmission of images, text and sound was demonstrated using piezo-electric transducers (PZT) at 2KB/s data rate. Efforts are under way to increase data transmission rate of the communication system through algorithmic improvements in GNURadio protocol, and through optimization of hardware resources. Algorithmic improvements will include better design of automated gain controller to potentially reduce the time needed to compensate amplitude reduction of the demodulated signal. Other improvements under current study include design of decimation algorithm which tracks the rising

and falling edges of the received pulse. Presently, the challenge in decimation is that the receiver is not synchronized with the transmitter

References

Argonne National Laboratory (2018), “Realizing a Pipe Dream,” https://www.anl.gov/articles/realizing-pipe-dream

Bakhtiari, S, Chien, H.T., Heifetz A., Elmer, T.W (2018) “Nondestructive Testing Research and Development Efforts at Argonne National Laboratory: An Overview,” Materials Evaluation 76 (7), 911-920.

Chakraborty S.,. Saulnier G.J,. Wilt K.W, Curt E.,. Scarton H. A, Litman R.B., (2015) "Low-power, low-rate ultrasonic communications system transmitting axially along a cylindrical pipe using transverse waves," *IEEE Transactions on Ultrasonics*, vol. 62, no. 10, pp. 1788-1796,

Heifetz A., Huang X., Ponciroli R., Bakhtiari S., Vilim R.B. (2018) “Transmission of information by acoustic communication along metal pathways in nuclear facilities,” Digital Environment for Advanced Reactors Workshop, Argonne National Laboratory. https://gain.inl.gov/SiteAssets/DigitalEnvironmentPostersandDemos/Transmission_of_Information_by_Acoustic_Communication_ANL.pdf

Heifetz A., Huang X., Ponciroli R., Bakhtiari S., Vilim R.B. (2018) “Acoustic Communication over Metal Pipes in Nuclear Facilities,” submitted to NPIC&HMIT

Heifetz A., Huang X., Shribak S., Bakhtiari S., Saniie J., Vilim R.B., (2018) “Analysis of Achievable Rates of Communication,” Argonne National Laboratory ANL-18/27, August 31.

Heifetz A., Young J., Huang X., Bakhtiari S., Saniie J., Vilim R.B, (2018), “Acoustic Channel Link Models for Digital Communication Protocols,” ANL-18/25, August 15.

Heifetz A., Ponciroli R., Huang X., Wang B., Saniie J., Bakhtiari S., Vilim R.B. (2018) “Ultrasonic Link Model Development,” Argonne National Laboratory ANL/NE-18/7, March 30.

Heifetz A., Bakhtiari S., Huang X., Ponciroli R., and Vilim R.B. (2017) “First Annual Progress Report on Transmission of Information by Acoustic Communication along Metal Pathways in Nuclear Facilities,” Argonne National Laboratory ANL/NE-17/30, September 30.

Heifetz A., Bakhtiari S., Vilim R.B. (2017) “Development of System Performance Models,” Argonne National Laboratory ANL/NE-17-22.

Heifetz A. and. Vilim R.B., (2017) “Eigendecomposition model of resistance temperature detector with applications to S-CO 2 cycle sensing,” Nuclear Engineering and Design 311, 60-68.

Korsah K., Kisner R.A., Britton Jr. C.L., Ramuhalli P., Woodan D.W., Anheier N.C., Diaz A.A., Hirt E.H., Vilim R.B., Chien H.T., Bakhtiari S., Sheen S.H., Gopalsami S., Heifetz A., Tam S.K., Park Y., Upadhyaya B., Stanford A. (2017) “Assessment of sensor technologies for Advanced Reactors,” Pacific Northwest National Laboratory PNNL-SA-132062.

Wang B., Saniie J., Bakhtiari S., and Heifetz A. (2017) "Architecture of an ultrasonic experimental platform for information transmission through solids," 2017 IEEE International Ultrasonics Symposium (IUS), Washington, DC, pp. 1-4.

Nuclear Science and Engineering (NSE) Division
Argonne National Laboratory
9700 South Cass Avenue, Bldg. 208
Argonne, IL 60439

www.anl.gov